Experimental and Numerical Study on the Thermal Performance of Earthbag-wall Units Incorporated with Phase Change Materials

Mahmoud Murtala Farouq, Parham A. Mirzaei, Carlos Jimenez-Bescos, Saffa Riffat

PII: S2352-7102(24)00874-X

DOI: https://doi.org/10.1016/j.jobe.2024.109306

Reference: JOBE 109306

To appear in: *Journal of Building Engineering*

Received Date: 5 September 2023

Revised Date: 26 February 2024

Accepted Date: 10 April 2024

Please cite this article as: M.M. Farouq, P.A. Mirzaei, C. Jimenez-Bescos, S. Riffat, Experimental and Numerical Study on the Thermal Performance of Earthbag-wall Units Incorporated with Phase Change Materials, *Journal of Building Engineering*, https://doi.org/10.1016/j.jobe.2024.109306.

Experimental and Numerical Study on the Thermal Performance of Earthbag-wall Units Incorporated with Phase Change Materials

Mahmoud Murtala Farouq[a,c], Parham A. Mirzaei[b], Carlos Jimenez-Bescos[d], Saffa Riffat[a]

[a]Architecture & Built Environment Department, University of Nottingham, University Park, Nottingham NG72RD, United Kingdom

[b]Department of Civil and Architectural Engineering, Aarhus University

[c]Kano University of Science and Technology, Wudil, Nigeria

[d] Westminster Business School, University of Westminster, London, UK

Abstract

The demand for temporary housing for refugees and displaced communities has led to the exploration of earthbag buildings. While these structures are affordable and sustainable, they often struggle with thermal discomfort in extreme climates. This study aims to examine the integration of phase change materials (PCM) into earthbag walls to improve thermal performance. The research involved incorporating paraffin wax and microencapsulated PCM into scaled-down earthbag walls, with their performance evaluated in a controlled environment. The results were validated against a numerical simulation model developed in EnergyPlus. The study revealed significant thermal improvements with PCM integration. Wall-2, with paraffin wax A31, demonstrated a surface temperature reduction of up to 1.9℃, while Wall-3, with microencapsulation Inertek26, showed a decrease of 2.40℃ compared to the reference wall. A parametric analysis highlighted the importance of PCM layer thickness. Specifically, Wall-2 with a 6 cm paraffin wax layer achieved a maximum reduction of 4.0℃ compared to the base case. The study identified the transition temperature of PCM as a critical factor in thermal performance, with paraffin wax A31 emerging as the optimal choice. Placing the PCM layer on the interior surface of the wall was more effective than exterior placement. Overall, PCM integration in earthbag walls offers a promising solution to enhance thermal comfort in temporary housing, addressing the critical needs of refugees and displaced communities. This research fills existing gaps in thermal comfort in temporary housing and demonstrates the potential of PCM as an innovative passive design strategy.

Keywords: Phase change material; Earthbag wall; Indoor environment; Temporary housing; EnergyPlus; Climate chamber;

Nomenclature

ω_R	Total uncertainty
k	Thermal conductivity (W/mK)
A	Area of the wall (m^2)
ΔT	Temperature difference between the wall surfaces (℃)
l	Wall thickness (m)
q	Rate of heat transfer (W)
h_c	Convective heat transfer coefficient W/m^2K
T_b	Temperature of the inner surface (℃)
T_i	Temperature of the indoor air (℃)
v_w	Air speed (m/s)
TL	Time lag (hr)
$T_{i,max}$	Maximum inner surface temperature (℃)
$T_{o,max}$	Maximum outer surface temperature (℃)
f	Decrement factor
T_i^j	Temperature at node i and time step j (℃)
Δt	Time step (min)
ΔX	Finite difference layer thickness (m)
Cp	Specific heat of the material ($\frac{kJ}{kg}.K$)
ρ	Density (Kg)
c	Space discretisation constant
(α)	thermal diffusivity of the material (m^2/s)
Fo	Fourier number
$h(T)$	Enthalpy node as a function of temperature (Kj/Kg)

r	Correlation coefficient	

Abbreviation

P	PCM
EP	Expanded perlite
G	Expanded graphite
PEPG	Composite PCM
Wall-1 (baseline)	Reference wall
Wall-2 (WA31)	Wall with PCM composite
Wall-3 (WInk26)	Wall with Inertek26 microencapsulated PCM
Wall-4 (WA28)	Wall with microencapsulated PCM
Wall-5 (WInk23)	Wall with Inertek23 microencapsulated PCM
PCM-E	PCM-integrated earthbag unit
FAC2	Fraction within a factor of two
FB	Fractional bias
NMSE	Normalised mean square error

1. Introduction

Fossil fuels are the most widely used source of energy for housing worldwide [1]. Fossil fuel usage has caused many socioeconomic and environmental problems, including fossil fuel depletion, greenhouse gas emissions, global warming, air quality deterioration, oil spills, and acidic rain [2]. The building sector has experienced ongoing and rapid growth, accounting for 30–40% of the total global primary resource use [3]. In tropical developing countries with high temperatures and strong solar gains, the main part of the energy demand related to the cooling of spaces in buildings is exacerbated [4].

Despite the need to provide a healthy and comfortable environment for housing occupants, such goals are yet to be achieved globally for temporary housing owing to many circumstances, such as fuel poverty [5], forced displacement [6], and high levels of insecurity [7]. This situation has resulted in a global need for temporary housing to accommodate millions of refugees and displaced individuals [8].

An estimated 15 million individuals are internally displaced in Nigeria alone [9] due to various causes such as coercive movements, civil wars, insurgency, and ethnic discrimination by government policies [10]. Such displacement causes great suffering because internally displaced persons (IDPs) lack access to suitable shelters, food, and healthcare. One of the main concerns for such housing is their poor indoor environmental conditions, as relocated individuals are often displaced to inhospitable regions that are barely accessible [11]. [12].

Earthbag buildings emerged long ago as a practical temporary housing solution because they are inexpensive, quick, and simple to construct using natural components. Earthbag housing can be easily decomposed, and the materials can be returned to nature with a minimum human-related environmental footprint [13]. Furthermore, earthbag buildings are more thermally comfortable than burnt or concrete bricks [14]. However, few studies have focused on the performance of earthbag buildings in hot and dry climates. Rincón et al. (2019) [15] revealed that a high-inertia earthbag building with solar protection and night ventilation effectively mitigates thermal discomfort. Additionally, Wesonga et al. (2021) [16] studied and compared the thermal performance and total life cycle costs (LCC) of earthbag walls and burnt brick walls in Uganda's hottest region and found that the thermal performance of earthbag housing was better than that of a brick wall, resulting in a lower annual energy consumption and cost savings of up to 83.2%. Despite these positive results, some studies have argued that earthbag buildings are not thermally comfortable even when another technological system is incorporated, such as a radiative cooling system [17] and that they have lower insulating effectiveness than dual glasses [18]. A possible solution is to couple the earthbag with other materials, such as straw layers [19]. Traditional building insulation materials have mainly been applied in thick or multiple layers to achieve greater thermal resistance, creating heavier load bearing and complexity [20]. To address this, passive strategies such as integrating energy storage are needed, which can enhance thermal resistance by shifting the energy demand from peak to off-peak periods. This approach buffer temperature fluctuations but also improves the indoor climate, particularly in temporary housing under harsh climatic conditions [21]. As a commonly utilised storage technology, phase change material (PCM) can potentially reduce thermal discomfort in buildings [22], [23]. PCM have strong thermal properties and high latent heat capacity, making them excellent thermal storage media that can significantly improve energy efficiency [24].

Phase change materials can be incorporated into building components in different ways; one of the simplest methods is direct incorporation. However, the direct incorporation of PCM in buildings may lead to leakage as the PCM changes from solid to liquid or vice versa during the charging and discharging periods [25]. To address this limitation, cross-linked polymer matrix, a porous mineral material or expanded graphite or perlite which have the virtue of shape stability have been used to

encapsulate PCM [26]. [27] fabricate a PCM composite made by impregnating paraffin into hydrophobic coated expanded perlite (EPO) granules using two methods, direct impregnation, and vacuum impregnation. The stability of this composite was compared with that of a paraffin/uncoated expanded perlite (EPW) phase change composite. Results showed that the paraffin/EPW composite had significant leakage PCM), while no PCM leakage was observed for the paraffin/EPO composite. [28] reports on a leakage test using the oozing circle method to investigate the leakage condition in the expanded perlite/paraffin composites. The results showed that no leakage occurred in composites containing 31.5 mass% of paraffin. [29] developed PCM composite using octadecanol (OC) as PCM and expanded perlite (EP) and graphite using vacuum impregnation method. Leakage-proof properties of the composites are investigated, and it is found that adding expanded graphite (EG) with a mass fraction of 5%, 10%, or 15% weakens leakage phenomena.

EnergyPlus, an advanced simulation software, plays a crucial role in evaluating these PCM integration strategies. Researchers have employed EnergyPlus to assess PCM impact on building thermal performance. Cui et al. (2015) [30] prepared a macro-encapsulated lauryl lightweight aggregate (LA-LWA) for thermal energy storage concrete (TESC). The experiment was conducted in a TESC room and validated using an EnergyPlus simulation engine. The results showed that the PCM-integrated walls exhibited the best thermal and energy performance. Ramakrishnan et al. (2017) [32] investigated the thermal enhancement of PCM integrated cementitious composites board (PCMCB) for building walls. The study used experimental and numerical simulations with EnergyPlus v8.5 software and found that integrating PCM reduced indoor temperatures by up to 4.43 °C during summer days. Combining PCMCB with night ventilation further reduced peak indoor temperatures by up to 3.4 °C. Many other researchers have used EnergyPlus to conduct simulations of phase change materials for building thermal performance [33],[34],[35].

The use of PCM in conventional buildings, such as wallboards [36], bricks [37], and concrete [38], has been extensively studied, as the literature showed above. However, the use of PCM in vernacular buildings such as adobe rammed earth, cob buildings, and earthbags has not been explored much in the literature. Few studies focused on this research area. For example, Serrano et al., (2013) [39] optimised the formulation of stabilised rammed earth with 10% PCM, resulting in a 9.3% increase in heat capacity and a 23.5% decrease in thermal conductivity. Gounni & Louahlia, (2020) [40] demonstrated that integrating PCM in a cob house reduced the annual temperature oscillation and heating loads compared to conventional building materials. Zaineb et al. (2020) [41] evaluated the energy saving potential of clay-straw-wall integrated with PCM in Morocco's Draa-Tafilalet Region. They found that the peak heat flux of the straw-clay-inner-PCM wall decreases by 31.95%, while straw-clay-outer-PCM only drops by 26.5%. A study conducted by Toufigh and Samadianfard, (2022) [42]

showed that using PCM in rammed earth helped control temperature variations. In another study, 'M'hamdi et al., (2022) [43] found that using PCM was more efficient for cooling in the arid climate and heating in the sub-arid and Mediterranean climates, with the rammed earth envelope showing a maximum energy reduction of 10.7%. This study addresses significant research gaps in the field of thermal comfort in temporary housing and the integration of phase change materials (PCM) into building practices. Currently, there is limited research available on thermal comfort considerations specific to temporary housing, especially in hot climates. Additionally, the incorporation of PCM into building materials, particularly in the context of Nigeria's climate, has not been adequately explored. Furthermore, the potential benefits of utilizing modern passive energy storage materials, like PCM, are often overlooked in traditional vernacular building methods. The thermal properties and characteristics of earth buildings with PCM have also not been extensively studied. In light of these limitations, this study investigates the incorporation of modern commercial technologies, specifically PCM, into earthbag building practices to alleviate thermal discomfort in severe climates, particularly for temporary housing such as refugees and internally displaced individuals. The lack of research on strategies to mitigate thermal discomfort in temporary housing, especially in hot climates, poses potential risks to vulnerable occupants, particularly children. Thus, the current study proposes a passive strategy involving PCM as an innovative and sustainable solution for addressing thermal discomfort challenges in temporary earthbag housing. Previous research has shown promising results, indicating that the integration of PCM into earthbag units can lead to a reduction in inner surface temperatures by as much as 4.1℃ [44]. To build upon these findings, an experiment involving a 1-zone building with a PCM-integrated earthbag wall was conducted and subsequently validated through numerical simulations. Various earthbag walls were manufactured with and without PCM, and their thermal performance was evaluated within an environmental chamber. The experimental results were corroborated using an EnergyPlus simulation model. Consequently, a parametric analysis was undertaken to identify the optimal PCM characteristics, including transition temperature, thickness, and placement. This comprehensive investigation seeks to contribute valuable insights into enhancing the thermal performance of temporary housing in hot, dry climates by leveraging PCM-integrated earthbag construction.

2. Method

The overall work on PCM-E wall development, thermal performance test, and numerical validation consisted of four main steps. The first step was the materials and preparation of the earthbag walls. This step involved selecting and preparing the materials that were used in constructing the earthbag wall. The second step was the experiment conducted on the earthbag wall in an environmental chamber that measured the thermal performance of the walls. Therefore, the performance of the wall was monitored within a 1-zone scaled building. The third step was validating the experimental result using developed numerical model of a 1-zone building. Performance evaluation was conducted to verify the validity of the numerical model develop, by comparing the inner surface temperature of the wall experimentally tested and the one numerically analysed. Finally, a parametric analysis was conducted to determine the suitable quantity of the PCM required for the PCM-E wall to achieve a better thermal comfort in their indoor environments.

2.1. Experimental Study

2.1.1. Materials and Methods

In hot climates like Nigeria, a PCM with a higher transition temperature option is preferable for reducing indoor temperature [45]. In this study, the selection process of PCM considered the comfort zone of the Kano state, the region for the experiment, which was determined to be between 23 and 32 °C [46]. Four (4) PCMs were utilised as thermal energy storage materials in a PCM-integrated earthbag unit. These PCMs included paraffin wax (A31 and A28) purchased from PCM Product Ltd, United Kingdom, and microencapsulated PCMs (Inertek26 and 23) obtained from MCI Technologies Company. For A31, a PCM composite was formed. The optimum amount of expanded perlite used to accommodate the PCM was determined to 50% of the PCM percentage weight. The percentage weight of the PCM for single earthblock as determined in our previous study was 0.39Kg per block [44]. The melted A31 PCM was inserted into the pores of the expanded perlite and 30g of expanded graphite via direct impregnation process, which allowed the PCM to be evenly distributed throughout the pores of the expanded perlite and graphite. The mixtures were kept in an oven at 50 °C for 3 h and then cooled at room temperature for 2 h. The PCM-composite PEPG was then formed and used for the PCM-integrated earthbag wall formation.. The Inertek26 was already microencapsulated and thus did not require a supporting material; therefore, it was directly incorporated into the PCM-integrated earthbag unit. However, A28 and Inertek23 were used only for parametric analysis. The phase change temperature and enthalpy of the A31, A28, Inertek26, and Inertek23 were analysed using differential scanning calorimetry (DSC). Sample of the PCMs (A31, A28, Inertek26, and Inertek23) weighing

between 5 and 10 mg were contained within a closed crucible and placed into a temperature-controlled DSC cell. A second crucible without sample was used as a reference. were tested under a nitrogen atmosphere, with a heating temperature range of 10–45°C, followed by a cooling temperature range of 45–10°C. The samples were tested at a ramp rate of 2°C/min. The thermophysical properties of the selected PCMs from the 'manufacturer's data sheet [47], [48], [49] are listed in Table 1.

Table 1. Technical data for the thermos-physical characteristic of Paraffin wax (A31 and A28) and Microencapsulated (Inertek26 and 23)

Product	**A31**	**A28**	**Intertek26**	**Intertek23**
Melting temperature℃	31	28	26 to 28	23℃ to 27
Phase change enthalpy (kJ/kg)	182	265	175	160
Specific heat capacity $(kJ/kg.K)$	2.22	2.22	2.0	2.0
Density (kg/m^3)	790	789	950	940
Thermal conductivity $W/(m.k)$	0.21	0.21	0.20	0.20
	Wall	Parametric analysis	Wall	Parametric analysis

2.1.2. Preparation of Earthbag Block

Twenty-four earthbag unit blocks were fabricated to construct earthbag unit test walls with and without PCM. A wooden frame for the earthbag block fabrication with dimensions of 400 mm × 250 mm × 100 mm (see Fig. A. 1) was prepared to enclose the mixture. The suggested optimal combination for making an earthbag block is 30% clay to 70% well-graded soil, as reported by Santos and Beirão (2017) [50]. The optimal soil content was determined based on a preliminary test. The mixture was carefully pressed into frame to prevent air gaps that could reduce the block strength. The quantity of A31 (in expanded perlite and graphite) and Inertek26 were mixed at 2.2% of the composition of the entire unit block mixture. Water was added to the mixture up to the point at which 10% moisture was achieved, as suggested by Geg, (2018) [51]. The mixture was thoroughly blended in a concrete mixer to achieve homogeneity.

Additionally, while pouring the mixture into the block mould, several tampings were made to ensure that the mixture in the bag was fully compacted. It was essential for consolidation that the tamping be moderate to avoid damaging the encapsulated PCM. Sixteen blocks were formed with PCM, including eight with the PEPG composite and the other eight with the Inertek26. The remaining eight out of 24 blocks were made without PCM and are referred to as baseline blocks. Fig. 1 shows the graphical criteria for preparing the mixes and block development.

Fig. 1 Earthbag block preparation

2.1.3. Wall Thermal Performance Testing

Three identical wall prototypes were built to assess earthbag-building test walls with and without PCM. Wall-1 (baseline) was constructed without PCM, whereas Wall-2 and Wall-3 were built with PEPG Composite and Inertek26, respectively. The prototype wall (see Fig. 2 a and Fig. 3 as a picture) was placed inside a controlled climatic chamber to form a 1-zone building. **Error! Reference source not found.**b shows a schematic layout of the thermocouples and the heat flux at the outer and inner surfaces of the PCM-integrated earthbag unit test wall and baseline wall. The tested wall was arranged with the upper portion constructed as a PCM wall and the lower portion constructed as a non-PCM wall. The tested wall was placed 600 mm from the climate-chamber door. A wooden barrier and expanded polystyrene board were used to separate the two walls and create an indoor space for testing (Room 1 and Room 2, as shown in Fig. 2a). The climatic chamber was programmed to simulate summer climatic conditions in Kano, Nigeria (see Section 3.1) to replicate the real conditions of the wall when tested outdoors. The climate chamber was divided into the outdoor temperature and the indoor space.

Additionally, ten k-type thermocouples with an accuracy of 0.5 °C were installed on the test wall, including five on the inner surface and five on the outer surface (refer to Fig. 2b). Moreover, two heat flux sensors with a calibration uncertainty of ±3% (k=2) were mounted on the wall to measure the heat flow rates. The relative humidity was set to 50% throughout the experiments. A thermocouple was placed in each indoor space to measure the indoor temperature (refer to Fig. 2c). All the sensors were connected to an automatic data acquisition system (DT80 DataTaker Data Logger) with a data recording frequency of 10 min. The data logger had a voltage-measurement accuracy of 0.1%. According to the experimental procedure, both the hot and cold chambers were initially maintained at 20 °C to ensure that the PCM remained in its solid form. The hot side was set with a Kano state profile temperature for three days. The experiment began once the hot chamber started to warm from the initial temperature to the first profile set temperature of 32 °C, causing a variable thermal boundary condition on the hot side of the PCM-earthbag wall. The experiment conducted over three days aimed to observe variations in the behaviour of the PCM-integrated earthbag unit within a climate chamber, simulating typical summertime conditions in Kano State. This period in April, representative of the region's summer climatic conditions, was selected to provide critical insights into weather patterns essential for accurate simulations. Focusing on April's peak temperatures was integral in evaluating the performance of the system under extreme conditions, a crucial factor in designing robust environmental systems.

278

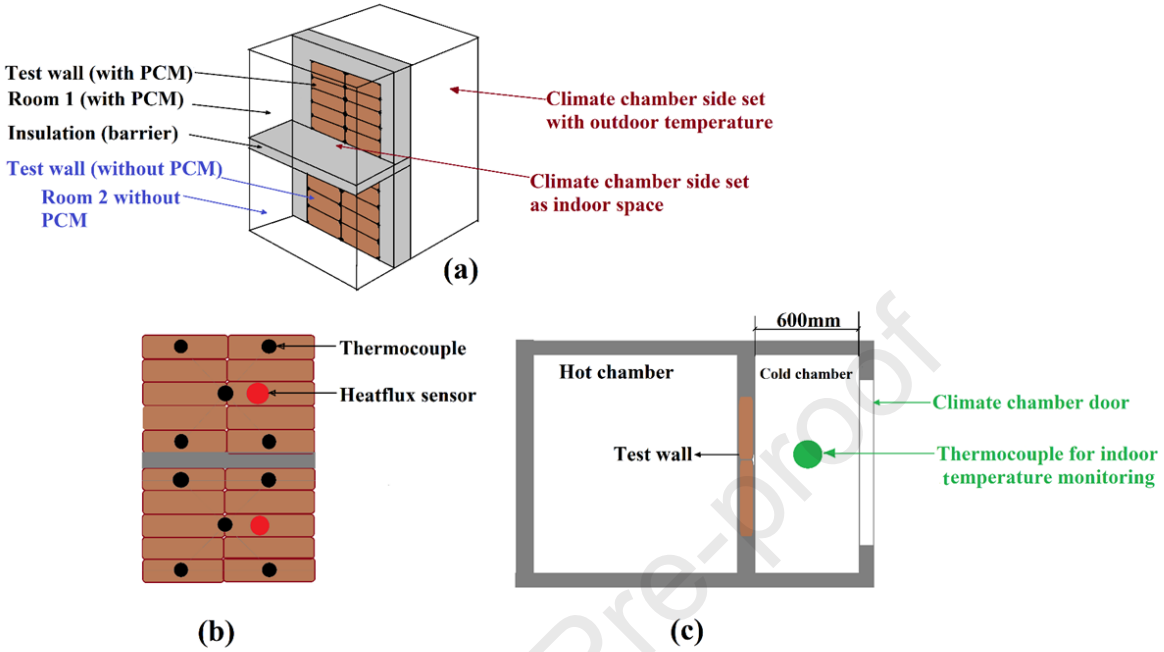

279

280 **Fig. 2** (a) Test walls prototype in climatic chamber (b) Schematic layout of thermocouples and heat flux at
281 outer and inner surface of walls (c) Top elevation of experimental arrangement

282

283

284

285 **Fig. 3** Tested prototype earthbag wall (with PCM upper and without PCM lower)

2.1.4. Uncertainty Analysis

To determine the accuracy of the experiment, an uncertainty analysis was performed. This study focused on measurements of the inner wall surface temperature and heat flow through the wall. Therefore, the uncertainties were derived from the random measurement of the errors of the K-type thermocouples and heat flux sensors. For the thermocouples, the accuracy was ±0.5°C, which means that the actual temperature was within ±0.5°C of the measured value. For the heat flux sensor, the calibration uncertainty was ±3% (k=2) according to the 's data sheet, which means there is a 95% chance that the actual heat flux is within ±3% of the measured value. Then, the uncertainty of the K-type thermocouples is ±0.3°C with an average temperature of 36.1°C, and the uncertainty of the heat flux sensors is ±0.68 W/m^2 with an average heat flux of 24.6 W/m^2. Thus, to calculate the percentage uncertainty of the measurement, we divided the total uncertainty by the measured value and multiplied it by 100%. Therefore, the percentage uncertainty of the K-type thermocouple was 0.7%, and that of the heat flux sensor was 2.8%. Now that we have individual uncertainties, we can calculate the combined uncertainty using the root sum of squares (RSS) method, as reported by Tokuç et al., (2015) [52] using Eqn. 1:

$$\omega_R = \left[\left(\frac{\partial R}{\partial x_1}\omega_1\right)^2 \left(\frac{\partial R}{\partial x_2}\omega_2\right)^2 + \cdots + \left(\frac{\partial R}{\partial x_n}\omega_n\right)^2\right]^{1/2} \quad (1)$$

where, ω_R is the total uncertainty in the result, R is the calculated result based on the uncertainties of the independent variables x_1, x_2 , x_3 …… x_n.

Hence, the total uncertainty of the experiment is 2.9%.

2.1.5. Thermal Conductivity Determination of Test Walls

To evaluate the thermal conductivity, an experiment was conducted using a controlled thermal chamber to determine heat transfer through the walls. The calibrated hot-box method was employed for the experiment, as outlined in the British Standard (BS 874-3.2, 1990). The aim was to establish a temperature difference between the two sides of the wall by placing a heat source (the hot side of the chamber) on one side and allowing heat to transfer through the wall layer to the other side (the cold side of the chamber refer to Fig. 2a). The temperatures of both wall surfaces were monitored under steady-state conditions. The temperature range chosen for the experiment was between 10

°C and 70 °C, which falls within the melting and solidification ranges of the selected PCMs. The data collected from the data logger through the heat flux sensors under steady-state conditions were used to calculate the thermal conductivities of the walls. The heat-flux sensitivity was 64.6 $V/W.m^2$, where the heat flux (q) was estimated by dividing the voltage by the sensor's sensitivity given in Eqn. 2 [53]:

$$q = \frac{voltage \times 1000}{64.6} \quad 2$$

Also, k as the thermal conductivity (W/mK) is determined by Eqn. 3 as follows:

$$k = \frac{ql}{A \times \Delta T} \quad 3$$

where A is the area of the wall (m^2), ΔT is the temperature difference between the wall surfaces (℃), and l is the wall thickness (m).

2.1.6. Heat transfer from surfaces

The convective heat transfer was used to calculate the amount of heat transfer between the inner surface of the wall and indoor air. This temperature difference typically has a low value; therefore, the radiative heat exchange between them can be neglected. Thus, the convective heat exchange can be calculated as using Eqn. 4 follows:

$$q = h_c A \ (T_b - T_i) \quad 4$$

where q is the rate of heat transfer from the inner surface to the interior environment, h_c is the convective heat transfer coefficient, T_b is the temperature of the inner surface, and T_i is the temperature of the indoor air. h_c can be adapted from the below Eqn 5 and 6 by applying either a linear or a power regression [54]:

$$h_c = 3.3v_w + 6.5 \quad 5$$

$$h_c = 9.5v_w^{0.48} \quad 6$$

where v_w is the air speed

The airspeed in the Kano state was measured using a National Geographic 256-Colour 5-in-1 Wireless Weather Station, and the measured values for three days are shown in Fig. B. 1. Measurements were taken during the summer period.

2.1.7. Specific heat capacity of earthbag wall

The specific heat capacity of earthbag wall is the amount of heat required to raise the temperature of a unit mass of the material by one degree Celsius (or one Kelvin). Below is the formula for calculation of specific heat capacity (*c*) of an earthbag wall:

$$c = \frac{Q}{m\Delta T} \quad (7)$$

Where *c* is the specific heat capacity of earthbag wall in Joules per kilogram per degree Celsius (*J*/(*kg*·°*C*)), *Q* is the amount of heat supplied to the wall in Joules (*J*), *m* is the mass of the of the wall in kilograms (*kg*), and Δ*T* is the change in temperature in degrees Celsius (°*C*).

2.1.8. Time lag and Decrement Factor

Time lag (TL) is the time when peak load is shifted to off-load. It can, therefore, be calculated using Eqn. 8 as the difference between the time at the maximum inner surface temperature ($T_{i,max}$) and the time at maximum average outer surface temperature ($T_{o,max}$) [55]:

$$TL = \tau T_{i,max} - \tau T_{o,max} \quad (8)$$

where $\tau T_{i,max}$ and $\tau T_{o,max}$τ are the times at the maximum inner and outer surface temperatures of the wall, respectively. The decrement factor (f) represented the ratio of the amplitude of temperature oscillation at the inner wall surface $T_{i,max}$ to that of the sol-air temperature $T_{o,max}$ [56]. The decrement factor can be calculated using Eqn. 9 below:

$$f = \frac{T_{i,max}}{T_{o,max}} \quad (9)$$

2.2. Numerical Model for Validation

2.2.1. PCM Modelling

EnergyPlus was employed in this study as building energy simulation software. A finite difference approach is included in EnergyPlus (EnergyPlus CondFD) to model materials with variable thermal properties using the enthalpy method [57]. As suggested by Tabares-Velasco et al., (2012) [58], a fully

implicit first-order scheme was employed in this study as the solution scheme. The first change process of the PCM is accounted for by a user-defined enthalpy temperature, as described in Eqn. 10 [59], and the enthalpy-temperature graph used for the simulation is illustrated in Fig. 7. The simulation was conducted with a time step of 3 min.

$$C_p \rho \Delta X \frac{\left(\boldsymbol{T_i^{j+i}} - \boldsymbol{T_i^j}\right)}{\Delta \boldsymbol{t}} = k_W \frac{\left(T_{i+1}^{j+1} - T_i^{j+1}\right)}{\Delta X} + k_E \frac{\left(\boldsymbol{T_{i-1}^{j+1}} - \boldsymbol{T_i^{j+1}}\right)}{\Delta \boldsymbol{X}} \quad 10$$

where k_W and k_E as thermal conductivities can be defined by Eqn. 11 and 12:

$$k_W = \frac{\left(k_{i+1}^{j+1} + k_i^{j+1}\right)}{2} \quad 11$$

$$k_E = \frac{\left(\boldsymbol{k_{i-1}^{j+1}} - \boldsymbol{k_i^{j+1}}\right)}{\boldsymbol{2}} \quad 12$$

where T_i^j is the temperature at node i and time step j , Δt is the time step, ΔX is the finite difference layer thickness, Cp is the specific heat of the material, and ρ is the density. Note that $k_i = k\left(T_i^{i+1}\right)$ if the thermal conductivity is variable.

In the CondFD algorithm, all elements are divided or discretised automatically using Eqn. 13, which depends on a space discretisation constant (c), the thermal diffusivity of the material (α), and the time step. Users can leave the default space discretisation value of 3 (equivalent to a Fourier number (Fo) of 1/3) or input other values [60].

$$\Delta x = \sqrt{c.\alpha.\Delta t} = \sqrt{\frac{\alpha.\Delta t}{F_0}} \quad 13$$

Equation 14 was integrated with the Enthalpy-temperature function (HTF), which was given by:

$$h = h(T) \quad 14$$

where $h(T)$ is the enthalpy node as a function of temperature.

The HTF developed an equivalent specific heat as a function of temperature ($Cp(T)$) at each time step for the PCM contained in the building as formulated by Eqn 15 [61]:

$$C_p^*(T) = \frac{h_i^j - h_i^{j-1}}{T_i^j - T_i^{j-1}} \quad (15)$$

where $C_p^*(T)$ is the specific heat as a function of temperature.

Moreover, to simplify the heat transfer across the wall model was assumed to be one-dimensional while the effect of convection within PCM was neglected.

3. Case Study

3.1. Location and Climate

Kano State, located in northern Nigeria [62], is an ideal location for studying the thermal performance of PCM-integrated earthbag units. The region experiences extreme temperature variations throughout the year, with hot and dry conditions in the summer, and cool and dry conditions in the winter [63]. Hence, using appropriate building materials and technologies is critical to creating comfortable living spaces in such environments. In this context, Kano state location meteorological year (RMY) weather data were employed, which were edited with outdoor measured real climatic conditions for a 1-zone building numerical model simulation that has been developed.

3.2. Validation

3.2.1. Model geometry and parameters

The developed case study aimed to investigate the effect of PCM-integrated earthbag unit walls to validate the experimental results. The model geometry (Fig. 4) employed in the simulation was designed to closely resemble the experimental setup (see Fig. 2) performed in an environmental chamber. As there is no code for an earthbag building, the literature was consulted to determine the dimensions and material characteristics, as shown in Table *2*. The model was constructed as a 1:2 scaled single room, two-story, and dual thermal zone, with a size of 800 mm × 400 mm and a height of 800 mm for each room. In the developed geometry, the top wall was used as wall with PCM (PCM composites or microencapsulated PCM) and a baseline wall (wall-1) were used as the tested walls. The tested walls with the PCM are wall-2 with A31 PCM (WA31) and wall-3 with Inertek26 PCM (WInk26).

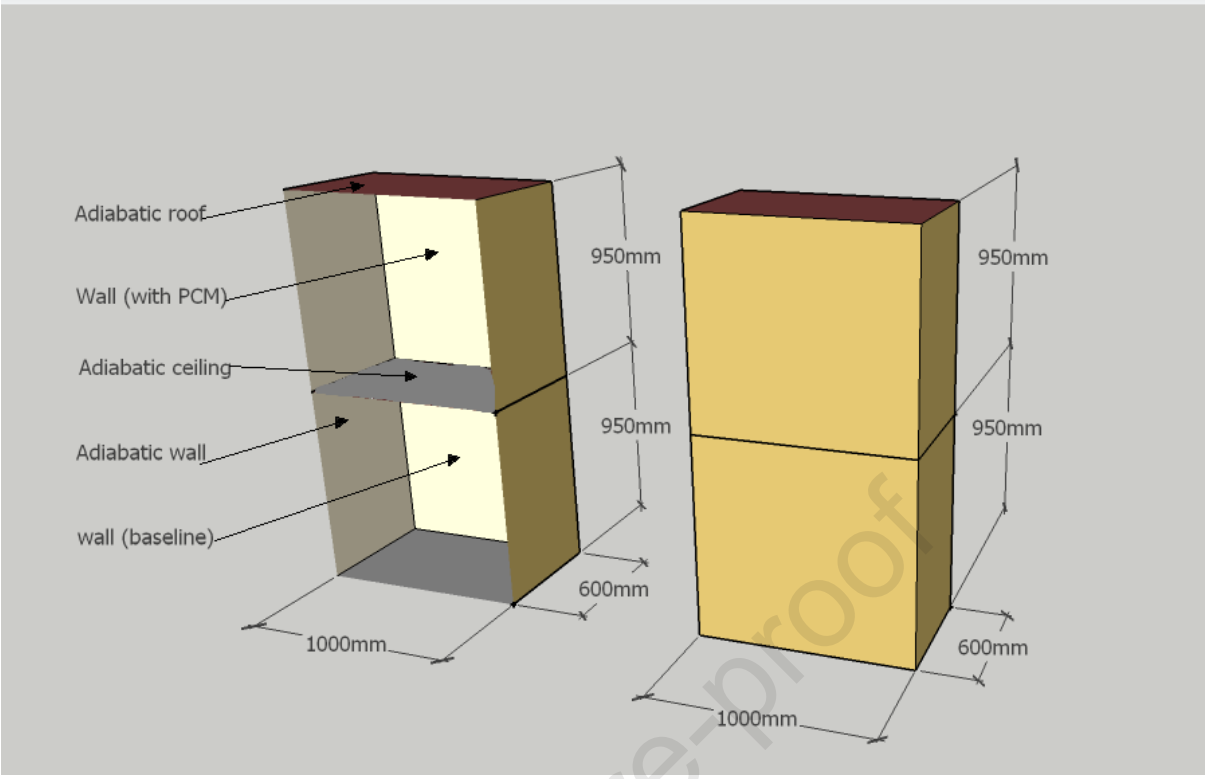

Fig. 4 Developed SketchUp model geometry

The first floor, ground floor, and all other walls were assumed to be adiabatic walls made from expanded polystyrene insulation (EPS) with a thickness of 100 mm. The simulation was performed for earthbag walls with and without PCM during summer. For validation, this study uses a graphical comparison recommended evaluation indices, as discussed in Section 3.2.1, and the mean error difference between numerical solutions and experimental data. The validation of the model is contingent on meeting specific criteria, as outlined in reference [64]. These criteria include achieving a less than 10% validation error between the numerical solutions and experimental data and meeting acceptable absolute mean errors. Specifically, an absolute mean error of less than 2°C is recommended for the inner or outer surface temperatures.

Table 2 Numerical model materials properties [15], [65]

System	Thickness m	Conductivity (W/ m. K)	Density (kg/m^3)	Specific heat (J/kg . K)
Earthbag wall	0.25	1.83*	2190	1000

Earthbag wall with A31 composite	0.25	0.74*	1980*	2100*
Earthbag wall with Inertek26	0.25	0.43*	1800*	2050*
Floor (expanded polystyrene insulation (EPS) board)	0.075	0.037	2390	1650
A31 PCM layer	0.01	0.21	790	2.22
Inertek26 PCM layer	0.01	0.20	950	2.00
Slab (expanded polystyrene insulation (EPS) board)	0.075	0.037	2300	1650

414 *Calculated from the experiment conducted

415 **3.3. Parametric Analysis**

416 Once the EnergyPlus models was validated with experimental data, the developed model was used
417 for a parametric analysis by converting the PCM quantity accumulated within a single wall to a layer.
418 The important of this is to determine the optimum PCM quantity that can give optimum thermal
419 comfort. The thickness of PCM was found to be 0.001m for A31 and 0.002m for Inertek26 PCM. This
420 was found using PCM equivalent method [30] (see Appendix C). The methodological approach for
421 transforming PCM composites and Microencapsulated PCM into a PCM layer is depicted in Fig. 5.
422 Additionally, Figure. 5 presents a detailed illustration of the PCM-E wall configuration employed for
423 the parametric analysis conducted in this study. Prior to undertaking the parametric analysis, a
424 thorough comparative evaluation of the simulated data for both the PCM composite and the
425 resultant PCM layer was performed. This preliminary step was critical to confirm the validity of the
426 equivalent method application. However, for validation 1cm layer thickness was used for both A31
427 and Inertek26 PCM. To facilitate a comprehensive parametric analysis, additional PCMs, specifically
428 A28 and Inertek23, were incorporated. The study systematically explores varying thicknesses of PCM
429 layers, ranging from 1 cm to 7 cm, to ascertain the optimal thickness for effective performance of the
430 PCM. This detailed investigation contributes significantly to our understanding of PCM behaviour in
431 energy-efficient building design. The thermophysical properties of the PCMs used in the simulation
432 are tabulated in Table 1.

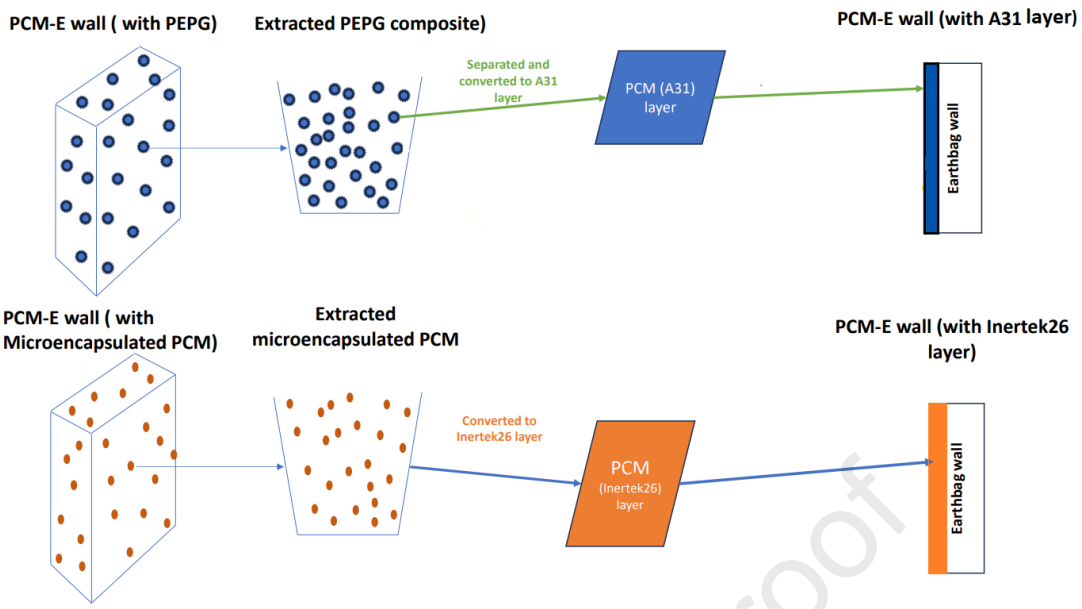

433

434 **Fig. 5** Conversion and extraction process of PCM composites and Microencapsulated PCM to PCM layer

435 The PCM enthalpy and DSC curve of the PCMs are experimentally found and presented in this section.
436 The DSC results in this study provide important information about the thermal properties of four
437 different PCMs: A28 and A31 paraffin wax, Inertek26 and Inertek23 powder. The DSC measurements
438 include enthalpy, peak temperature, and onset temperature. The DSC results are presented in Fig. 5
439 and Fig. 6. The results reveal that A28 paraffin wax has the highest enthalpy among the four PCMs,
440 indicating that it has the highest capacity for thermal energy storage. However, A28 paraffin wax also
441 has the lowest peak and onset temperatures, indicating that it changes phase at lower temperatures
442 than the other PCMs, which may limit its application in regions with higher ambient temperatures.

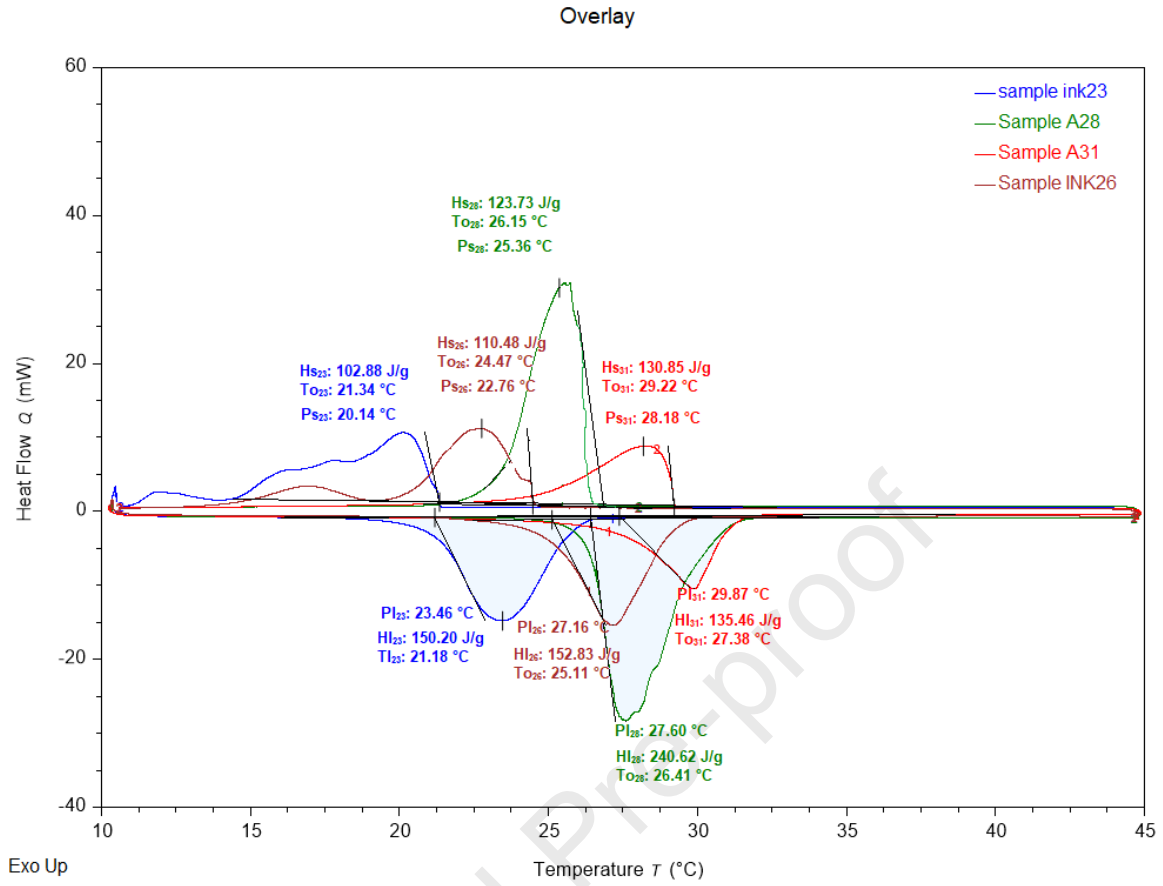

443

444 **Fig. 6** Phase transition temperature for A31, A28, Inertek26, and Inertek23 PCM

445 In contrast, A31 had the highest peak and onset temperatures among the four PCMs, making it
446 suitable for regions with higher ambient temperatures. However, A31 has the lowest enthalpy,
447 meaning it has a lower thermal energy storage capacity than the other PCMs. The DSC results suggest
448 that the choice of PCM depends on the desired thermal performance and the ambient temperature
449 range. A28 may be preferred for regions with lower ambient temperatures. The A31 may be
450 preferred for regions with higher ambient temperatures. The enthalpy temperatures curve of the
451 PCMs are shown in Fig. 7. A comparative analysis between the enthalpies obtained from the
452 manufacturer's data sheet as tabulated in Table 1 and those derived from experimental
453 measurements shown in Fig. 6 has been conducted to evaluate the consistency and reliability of the
454 provided data. Upon comparing the manufacturer's enthalpy data with the experimentally obtained
455 results, it is evident that the discrepancies between the two sets of data are relatively small. The
456 minor differences in enthalpy values can be attributed to various factors, including the influence of
457 experimental conditions, measurement techniques, and potential variations in material properties.
458 Despite these slight deviations, the overall agreement between the manufacturer's data and the

experimental measurements suggests a reliable representation of the PCM's enthalpy characteristics. The enthalpies obtained from the DSC are used as the input values in the EnergyPlus simulation.

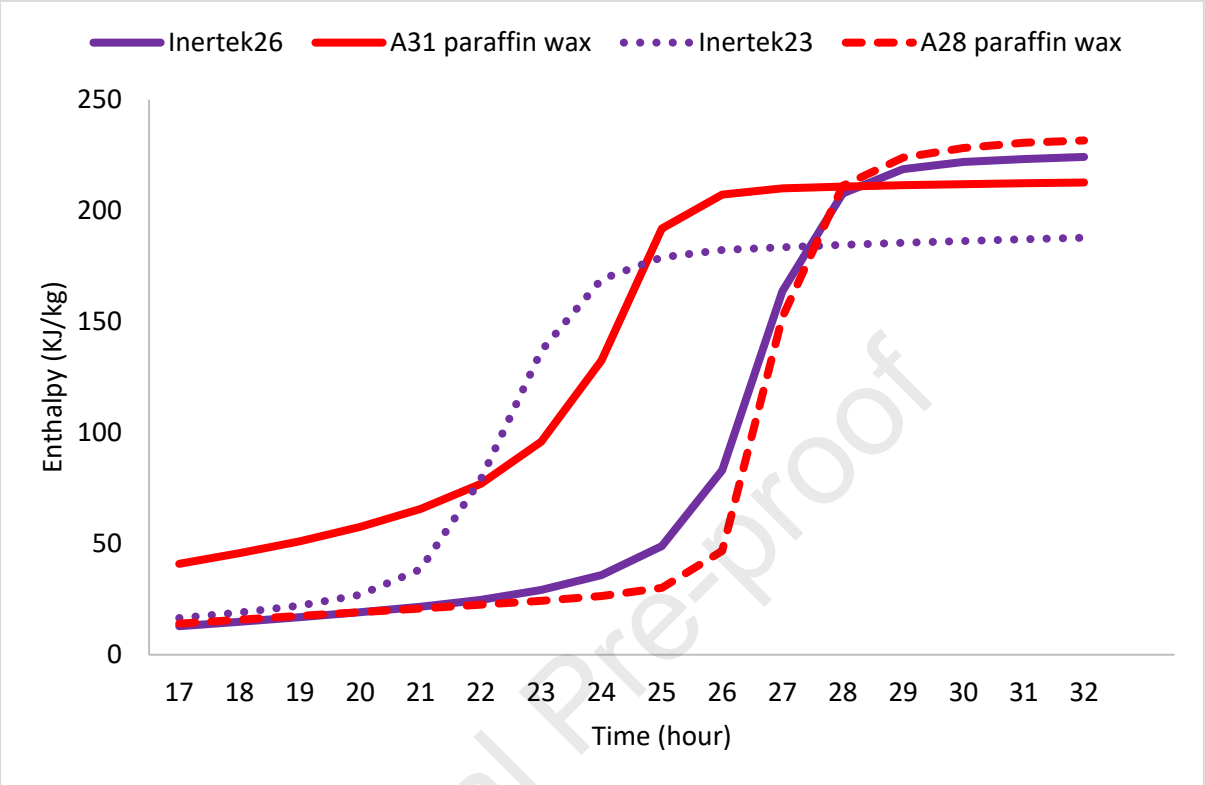

Fig. 7 Enthalpy temperature curves of Inertek26, 23 and A31, 28 PCM

3.4. Model validation metrics

To compare the experimental data and the simulation results, different metrics shown in Eqn.16, 17, 18, and 19 are used to evaluate the validation process, including the below used metrics: Correlation coefficient (r), fractional bias (FB), snormalised mean square error (NMSE), and fraction of predictions within a factor of two (FAC2).

$$r = \frac{n(\sum x_i y_i) - (\sum x_i)(\sum y_i)}{\sqrt{[n\sum x_i^2 - (\sum x_i)^2] - n\sum y_i^2 - (\sum y_i)^2}} \quad 16$$

$$FB = \frac{[y] - [x]}{([y] + [x])} \quad 17$$

$$NMSE = \frac{[(x_i - y_i)^2]}{[x][y]} \quad 18$$

$$FAC2 = \frac{1}{N}\sum_{i=1}^{N} n_i \; n_i = 1 \; if \; 0.5 \leq \frac{x_i}{y_i} \leq 2 \; else \; n_i = 0 \qquad 19$$

where y_i and x_i are the measured and computed values of a given variable for sample i, respectively. N is the number of data points used in the calibration process. The ideal value of the validation metrics for a complete agreement between two data series is 1 for r and FAC2 and 0 for FB and NMSE.

4. Validation of Experimental Result

4.1. Comparative Evaluation of The Experimental and Simulated Data (Embedded PCM (1cm layer equivalent) And 1cm PCM Layer)

The experimental and EnergyPlus simulation results were compared to validate the PCM-integrated earthbag unit wall of a 1-zone building. The assessment of the earthbag wall was based on the reduction in the inner surface wall. After using the validation metrics introduced in Section 3.4, the validation results were quite accurate, as shown in Fig. 8. The temperatures measured experimentally and numerically showed a similar pattern and corresponded well for all case studies. The temperature profiles of Wall-1 (baseline), Wall-2 (WA31), and Wall-3 (WInk26) (see Fig. 8) in the modelling results are relatively coherent. However, there are a few experimental measurement fluctuations, possibly due to material, experimental, or human error during the experimental setup. Wall-2 (WA31) is a composite phase change material that may cause temperature fluctuations due to uneven distribution and differences in its thermal conductivity. On the other hand, Wall-3 (WInk26) uses micro-encapsulated phase change materials that result in a more uniform distribution and less temperature fluctuation while also preventing PCM leakage, which can occur with composite materials. The differences in average temperature between the inner wall surface temperature with and without PCM for the experiment were found to be approximately 1.90℃ and 2.40℃ for WA31 and WInk26, respectively, which are close to the simulation results. The validation and absolute mean error analyses showed that the numerical solutions for all three walls were relatively accurate and successful, as the mean errors were well within the success criterion of less than 10%, as presented in Table 3. All maximum temperature differences were also less than 2 °C. The Fractional bias (FB), FAC2, NMSE, and r presented in Table 4 reveal acceptable ranges of metrics related to the simulation and experimental results when the PCM is integrated into the earthbag building. It can be stated that the criteria for both the inner and outer surface temperature of Wall-1 (baseline), Wall-2 (WA31), and Wall-3 (WInk26) are met. The NMSE and FB are nearly zero in all instances, while r ranges from

497 0.9 to 0.98 for the inner and outer surface temperatures across all cases.

498 Furthermore, the FAC2 values were all greater than 0.5, but less than 2, indicating good agreement
499 between the models. Overall, it can be concluded that the model tested with Wall-3 (WInk26)
500 performed better than all the other case studies. In general, the validation of the results was
501 successful for both earthbag buildings with and without PCM. The numerical solutions can, therefore,
502 be relied upon for further analysis and simulations. Consequently, it can be assumed that the PCM-
503 integrated earthbag unit model developed in this study can be utilised to predict the thermal comfort
504 of future earthbag buildings in different regions.

505 **Table 3** Discrepancies between numerical and experimental results

Wall	Maximum Inner temp difference (°C)	Maximum outer temp difference (°C)	Inner surface temp Mean Error (%)	Outer surface temp Mean Error (%)
Wall-1 (baseline)	1.0	1.6	0.9	2.3
Wall-2 (WA31)	0.6	1.5	0.7	1.4
Wall-3 (WInk26)	0.1	0.3	0.2	0.7

506

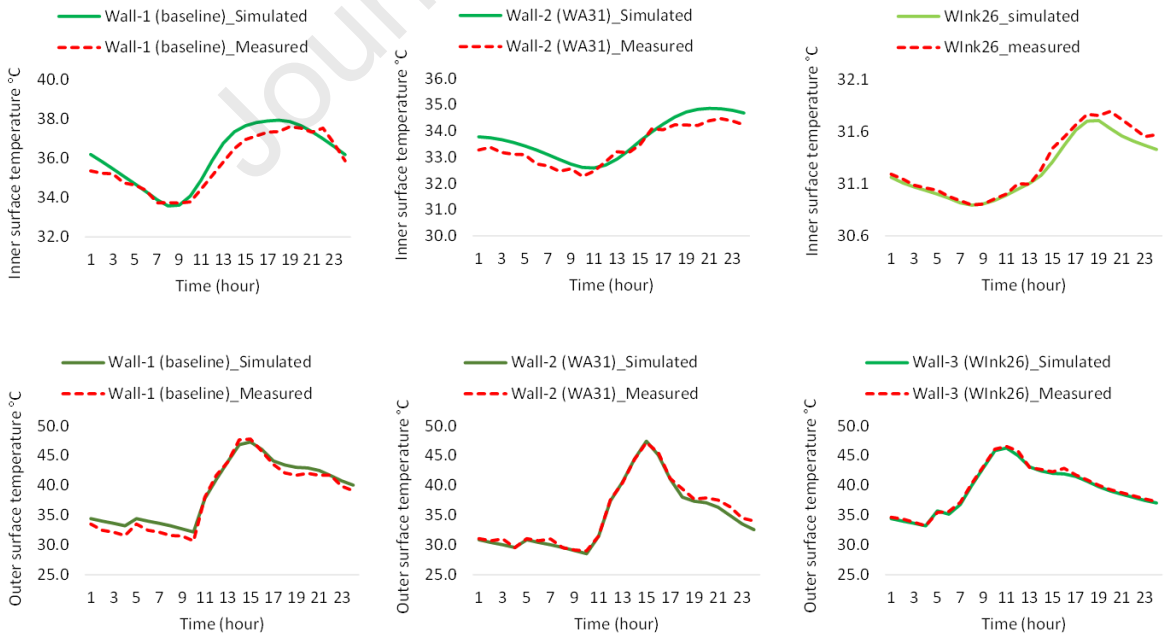

507

508 **Fig. 8** Temperature profile of Wall-1 (baseline), Wall-2 (WA31) and Wall-3 (WInk26)

509

Table 4 Validation metrics

Surface temperature	Fractional bias (FB)	NMSE	r	FAC2
Inner Wall-2 (WA31)	0.0005	0.0011	0.9540	0.9850
Inner Wall-3 (WInk26)	0.0001	0.0001	0.9803	1.4001
Inner Wall-1 (baseline)	0.0030	0.0061	0.9500	0.9404
Outer Wall-2 (WA31)	0.0009	0.0041	0.9000	0.9100
Outer Wall-3 (WInk26)	0.0003	0.0003	0.9670	1.1100
Outer Wall-1 (baseline)	0.0070	0.0081	0.9211	0.9286

5. Results and Discussion

5.1. Experimental results analysis

5.1.1. Thermal Conductivity of Earthbag Walls

As shown in Fig. 9, the steady-state condition of the wall is reached when the difference between the surface temperatures of the walls remains constant. The temperature differences between the hot and cold sides for Wall-1 (baseline), Wall-2 (WA31), and Wall-3 (WInk26) at steady state were 5.0℃, 6.6℃, and 8.6℃, respectively. Hence, the heat flux was found to be 23.3 W/m^2, 9.5 W/m^2, and 7.1 W/m^2, which was obtained from the data logger through the heat flux sensors at the steady state period. Therefore, the thermal conductivities of earthbag walls with and without PCM were measured in this study using three different test walls: Wall-1 (baseline), Wall-2 (WA31), and Wall-3 (WInk26). The results show that Wall-3 (WInk26) has the lowest thermal conductivity of 0.43 m^2K/W compared to Wall-2 (WA31) with a value of 0.74 m^2K/W, and Wall-1 (baseline) with values of 1.83 m^2K/W. As expected, the higher the quantity of PCM, the better the thermal performance [38],[66]. The quantity of PCM microencapsulated in volume was higher and distributed more uniformly than the PCM composite in the block. This is likely the primary contributing factor to the low thermal conductivity of Wall-3 (WInk26). The presence of PCM in the wall also reduces the heat transfer from the outer wall to the inner wall surface because the lower thermal conductivity of the PCM slows down the heat transfer rate. In hot climate regions, this characteristic of PCM is especially beneficial because it can potentially keep the inner surface temperature low [67]. Therefore, the earthbag wall with microencapsulated PCM demonstrated the best thermal conductivity in the experiment.

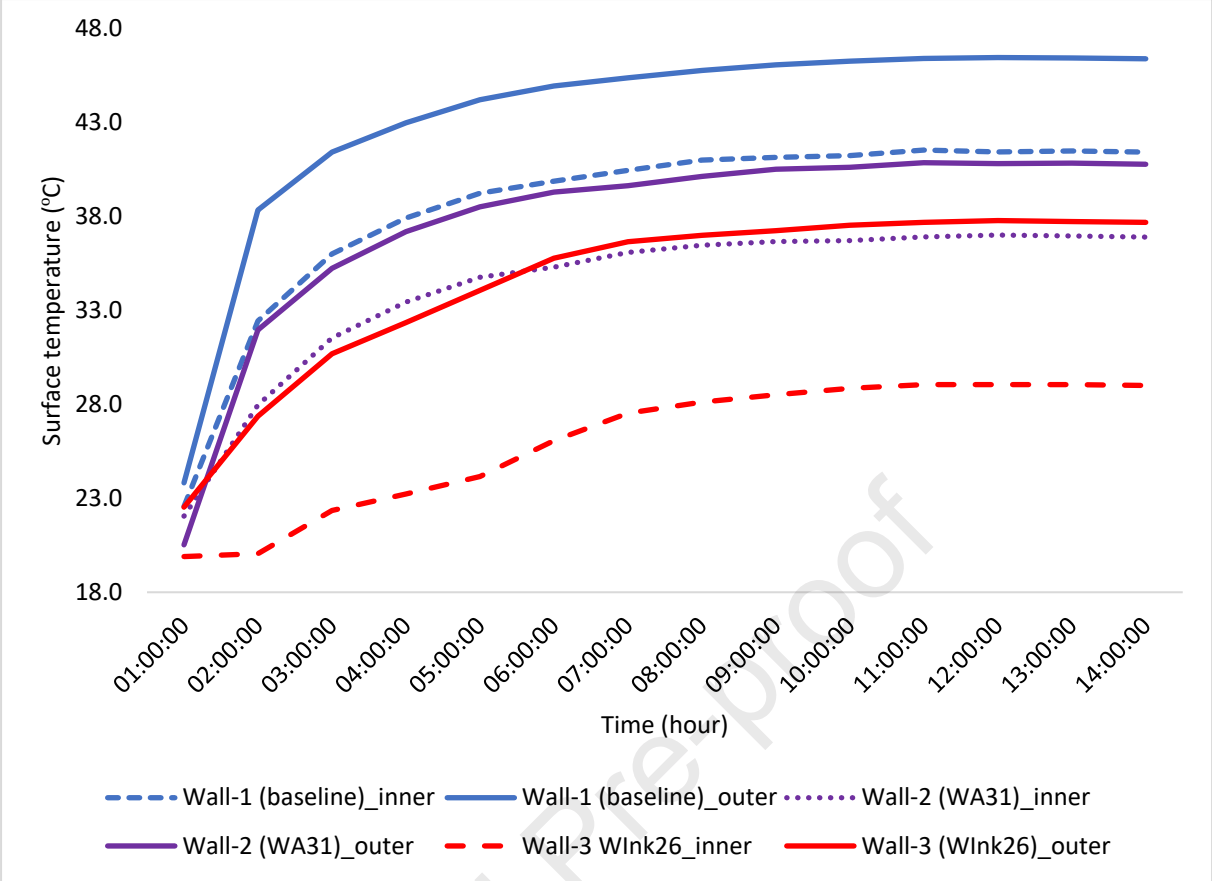

Fig. 9 Inner and outer surface temperatures of a walls at steady state

5.1.2. Wall Surface Temperatures

The inner surface temperatures of the walls are demonstrated over three days in April, as shown in Fig. 10. The Wall-3 (WInk26) have a more stable inner surface temperature than Wall-2 (WA31) and Wall-1 (baseline). This is due to the lower thermal conductivity of Wall-3 (WInk26), resulting in slower heat transfer to the inner surface temperature. The same pattern can be observed for the outer wall surface. In contrast, the wall without the PCM displays a higher temperature due to its higher thermal conductivity. Considering the melting temperatures of the PCMs used, it can be seen that they are ineffective, as the outdoor temperature during the first day of the experiment was above the melting temperature of the PCM. This causes an instant release of the stored heat to the inner surface, resulting in an increase in the inner surface temperature. This was also observed for the second and third days of the experiment. However, Wall-3 (WInk26) with the Inertek26 PCM, whose melting temperature is 26 °C, has the most stable inner surface temperature with a temperature variation of not more than 2 °C during the day. This results in a decrease in the maximum temperature amplitude compared to that of Wall-1 (baseline). The average temperature reduction between Wall-2 (WA31) and Wall-3 (WInk26), and Wall-1 (baseline) is 1.9℃ and 2.40℃. Fig. 10 shows that all internal surface

temperature values were higher than the phase transition temperature of the PCMs, rendering them ineffective in charging and discharging. This is likely due to the small quantity of PCM used, as adding a layer does not provide adequate thermal performance. Previous research has shown that if the PCM layer is too thick, it can act as an insulation layer, whereas if it is too thin, solidification may not occur, resulting in inadequate charging or discharging of the PCM [68]. Hence, incorporating more quantity of PCM is necessary to ensure the effectiveness of the earthbag unit wall.

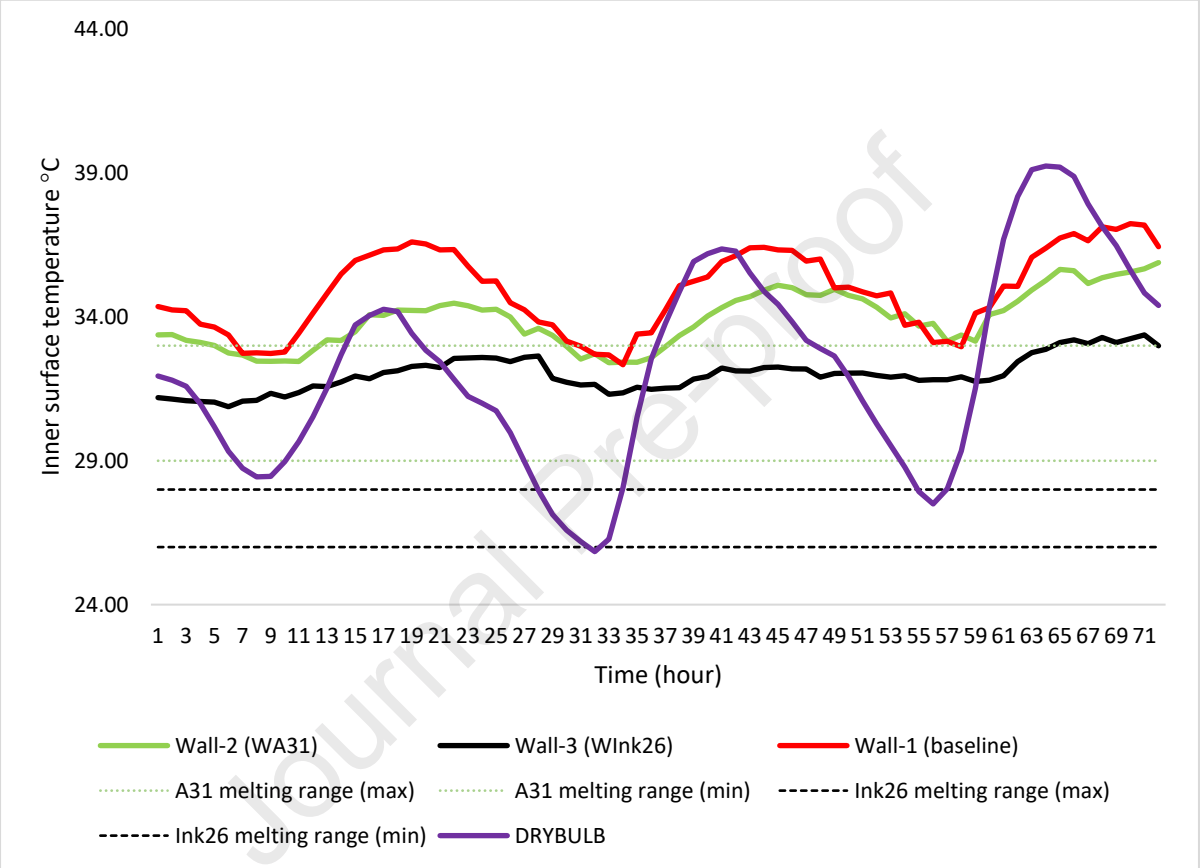

Fig. 10 inner surface temperatures of Wall-1 (baseline), Wall-2 (WA31) and Wall-3 (WInk26)

5.1.3. Time lag (TL) and Decrement Factor

The graph in Fig. 11 shows that the time lag of Wall-1 (Baseline) Wall-2 (WA31), andWall-3 (WInk26)varied throughout the experimental day. It is evident that the integration of the PCM leads to an increase in the time lag value, which is more pronounced in the Wall-3 sample (WInk26). In particular, the first and second days of the experiment showed time lags of 4 and 3 h, respectively. These values illustrate that the PCM integration can decrease the rate of heat penetration through the wall, which is crucial for maintaining lower temperatures inside the building. In contrast, the baseline wall recorded time lags of 2 h and 1 h for the first and second days, respectively, while a negative time lag of -1 h was observed on the third day. This lower time lag indicates that in the

absence of PCM, the rate of heat penetration through the wall is increased, leading to higher temperatures within the building. However, on the third day, a negative time lag was observed in Wall-2 (WA31), likely owing to the high outdoor temperature that caused the PCM within the wall to melt faster than usual, resulting in a high inner surface temperature and a lower time lag. The Wall-2 sample (WA31) behaved similarly to Wall-1 (baseline) on this day.

Fig. 11 Time lags of Wall-2 (WA31) and Wall-3 (WInk26)

Fig. 12 shows the wall decrement factor for Wall-1 (Baseline), Wall-2 (WA31) and Wall-3 (WInk26) over a three-day experiment. This factor is essential for mitigating the impact of external temperatures on the interior of earthbag buildings. Wall-2 (WA31) and Wall-3 (WInk26) had decrement factors of 0.94, 0.96, 0.95, and 0.89, 0.88, and 0.90, respectively, on the experiment's first, second, and third day. In comparison, the baseline wall had decrement factors of 0.98, 0.99, and 0.96 over the same period. The lower decrement factors observed for Wall-2 and Wall-3 suggest that these walls, which contain phase change material (PCM), offer better thermal performance than the baseline wall which does not contain PCM. The highest decrement factor for the baseline wall on all three days indicates a lesser ability to mitigate the impact of external temperature fluctuations. This is likely due to the absence of PCM, which when integrated into walls, can significantly improve the thermal inertia and thus, the overall thermal performance of the building. The lowest decrement factor for Wall-3 (WInk26) on all three days indicates better thermal performance, demonstrating

588 the effectiveness of PCM in enhancing the thermal regulation properties of the walls.

589

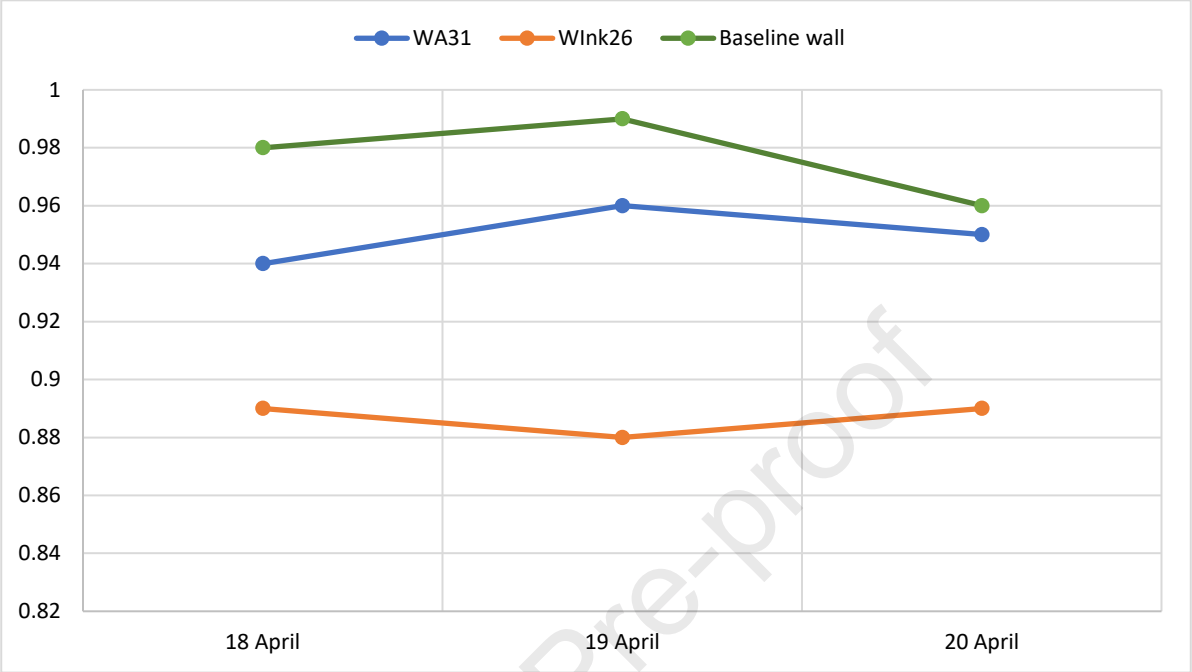

590

591 **Fig. 12** Decrement factor of Wall-2 (WA31) and Wall-3 (WInk26)

592 **5.1.4. Heat Flux and Heat Reduction Rate**

593 Monitoring the heat flux at the inner surface of an earthbag wall under the same outdoor climate
594 conditions revealed significant differences in thermal performance between walls with and without
595 phase change materials (PCMs). As shown in Fig. 13 Wall-1 (baseline) experienced its peak surface
596 heat flux at 18:00, whereas Wall-2 (WA31) and Wall-3 (WInk26) with PCM saw delayed peaks at 22:00
597 and 23:00, respectively, on the first day. This delay in heat transfer to the inner surface persisted
598 across the second and third days, with Wall-2 and Wall-3 delaying heat transfer by four and five
599 hours, respectively, compared to the baseline. The maximum heat flux for Wall-1 was 29.89 W/m^2,
600 significantly higher than 18.21 W/m^2 for Wall-2 and 10.22 W/m^2 for Wall-3, showcasing PCM's
601 effectiveness in reducing heat flux, with Wall-3 achieving a 63.76% reduction (see Table 5), the best
602 among the three.

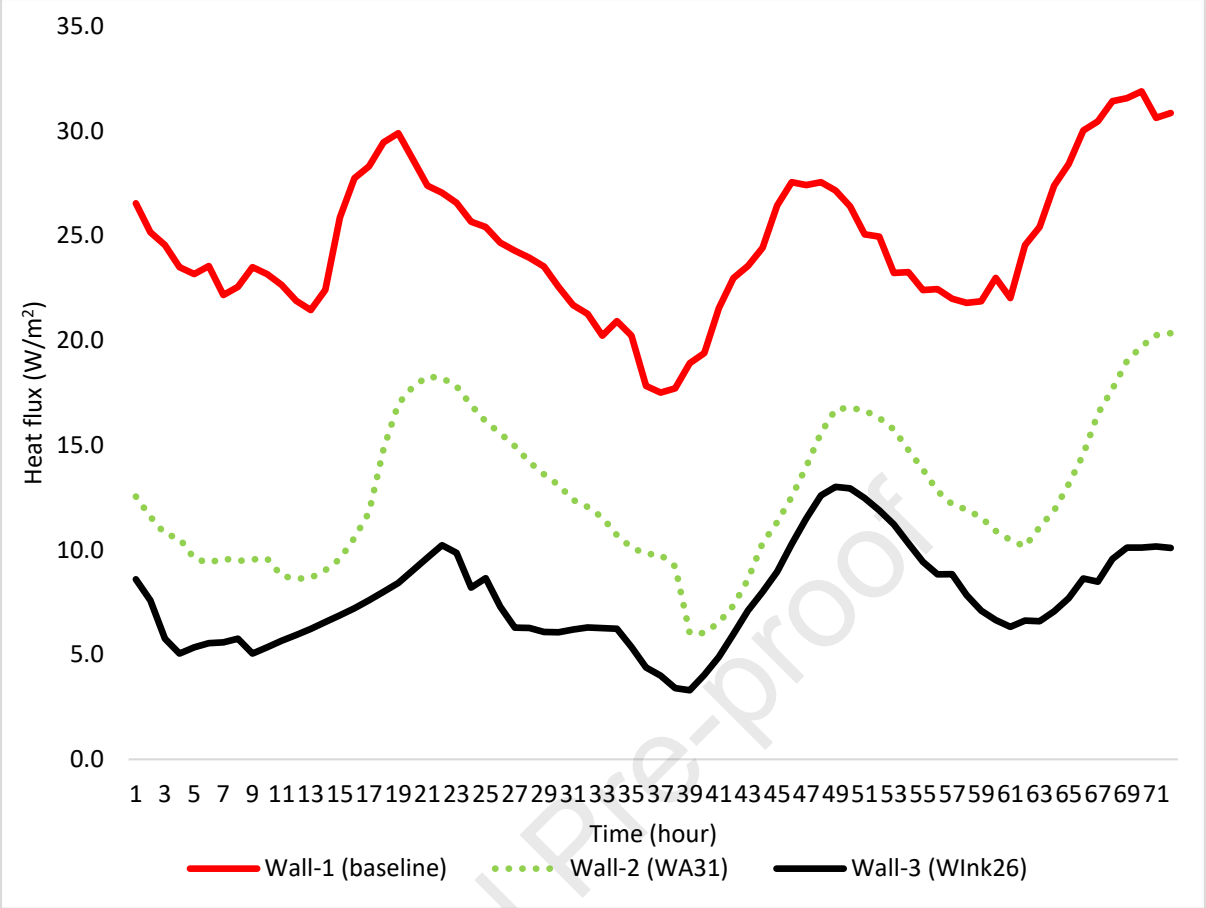

603

604 **Fig. 13** Stored heat flux in the Wall-1 (baseline), Wall-2 (WA31) and Wall-3 (WInk26)

605

606 **Table 5** Average heat flux reduction between reference, WA31, and WInk26 earthbag walls

Date	*Wall-1_(baseline)* W/m^2	Wall-2_(WA31) W/m^2	Wall-3_(WInk26) W/m^2	%Reduction Wall-2_WA31	%Reduction Wall-3_WInk26
04/18	29.89	18.27	10.22	40.22	68.09
04/19	27.55	16.64	13.01	41.09	54.76
04/20	31.56	20.34	10.65	36.71	68.42
			% Average	39.34	63.76

607

608 Integrating PCMs into the wall not only reduced the heat gain but also the energy required for cooling
609 or heating spaces. Wall-3 outperformed Wall-2 in heat transfer rates, confirming studies like Saxena
610 et al., (2020) [69] which highlighted the positive impacts of PCM in buildings. As depicted in Fig. 14
611 the microencapsulated PCM in Wall-3 resulted in lower heat transfer rates from the outer to inner
612 wall surfaces than Wall-2. Heat transfer values for Wall-1 over three days were 327.33 Wh/m^2,

156.96 Wh/m^2, and 196.91 Wh/m^2, significantly higher than Wall-2 (81.39 Wh/m^2, 78.08 Wh/m^2, and 84.27 Wh/m^2) and Wall-3 (58.96 Wh/m^2, 49.65 Wh/m^2, and 38.89 Wh/m^2). Wall-2 and Wall-3 showed remarkable reductions in heat transfer, with Wall-3 demonstrating superior performance with reductions of 268.37 Wh/m^2, 107.32 Wh/m^2, and 112.64 Wh/m^2 for the respective days, and percentage reductions in heat gain of 75.1%, 82.0%, and 50.3% for Wall-2, and 68.4%, 37.5%, and 57.2% for Wall-3. These findings underscore the effectiveness of PCMs, particularly Inertek26, in enhancing the thermal performance of earthbag walls by significantly reducing heat flux and transfer rates, thereby offering a sustainable solution to improve building energy efficiency. These findings are consistent with previous studies when PCM was incorporated into block wall (e.g., [69], [70], [54]).

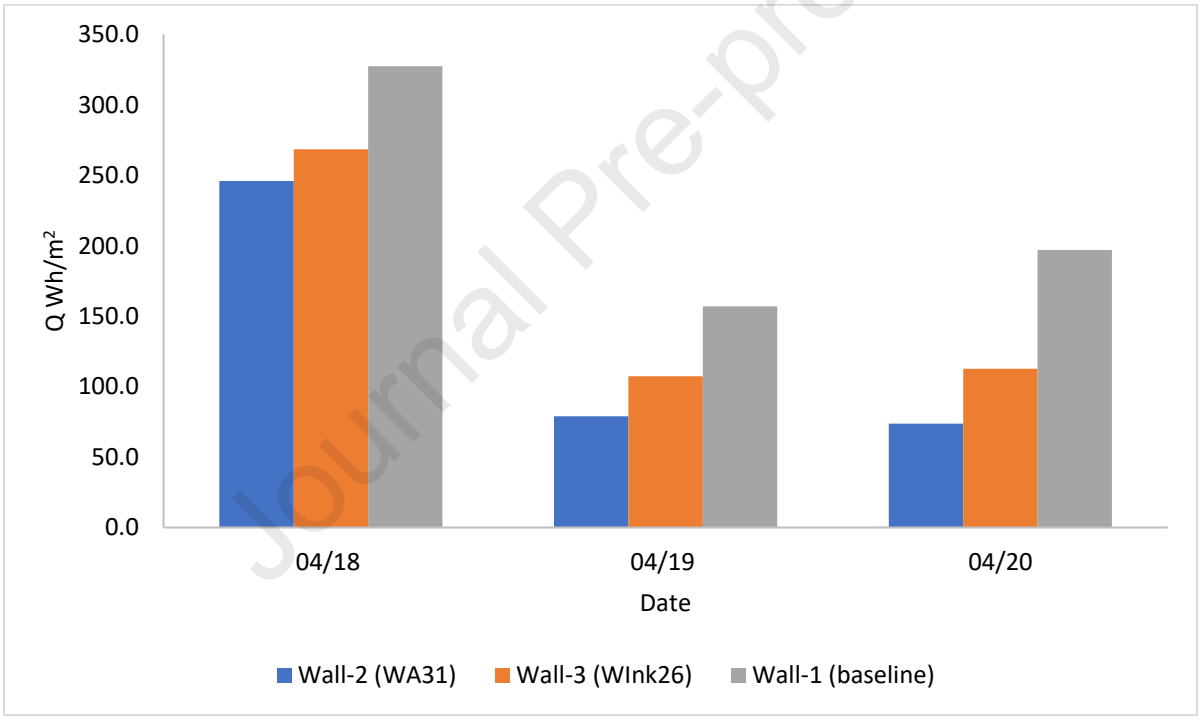

Fig. 14 Heat transfer reduction between the Wall-1 (baseline), Wall-2 (WA31) and Wall-3 (WInk26)

5.2. Simulation result

5.2.1. Result for Parametric Analysis

The parametric results considered four PCMs: paraffin wax (A31 and A28) and microencapsulated PCMs (Intertek 26 and 23). A31 and Intertek26 were used for experimental analysis and validation, while A28 and Intertek23 were not considered previously.

5.2.1.1. The Effect of PCM Transition Temperature

The transition temperature of the PCM is crucial for determining how much it undergoes a phase change, which affects the thermal performance of the walls with the PCM. The PCM will not change the phase or store thermal energy if the transition temperature is too low or too high. This section introduces various PCMs as layers in an earthbag wall to evaluate the effect of the PCM transition temperature.

Fig. 15 illustrates the inner surface temperatures of the earthbag building when utilising various PCMs, including A31 and 28, Intertek 26 and 23. Table 6 shows a significant surface temperature reduction for both PCMs compared with the baseline building without PCM. However, the PCM with a high transition temperature A31 exhibited the best temperature reduction, possibly due to outdoor temperature fluctuations. Even during summer nights, the outdoor temperature can be well below the PCM transition temperature. PCMA31 acts as an insulation material, preventing external heat from entering the indoor space of the earthbag. It also stores latent heat and releases it to the indoor space when the outside temperature drops. This can be seen in Fig. 15 for days 1, 2, and 3 for Wall-2 (WA31). For example, on April 19th (day 2), the outside temperature increased from 8:00 am to 5:00 pm (10 h). The earthbag wall receives excess heat energy that passes from the outside wall to the inner surface of the earthbag as conductive heat. The Wall-2 (WA31) accumulated this latent heat, which delayed the peak of the inner surface temperature. The temperature started rising at 11:00 am on April 19th and reached its peak at 1:00 am on April 20th, compared to the earthbag without PCM, which peaked at 9:00 pm. The other PCMs (A28, Inertek26, and Inertek23) also reduced the surface temperature compared with the baseline. However, they were above their PCM transition temperature for all days. This allows them to release the stored energy quickly and pass it to the indoor space of an earthbag building. Therefore, these PCMs do not work well as phase change

material. PCMA31 was selected as the optimum PCM for the earthbag building model in Kano state and other locations with similar climatic conditions.

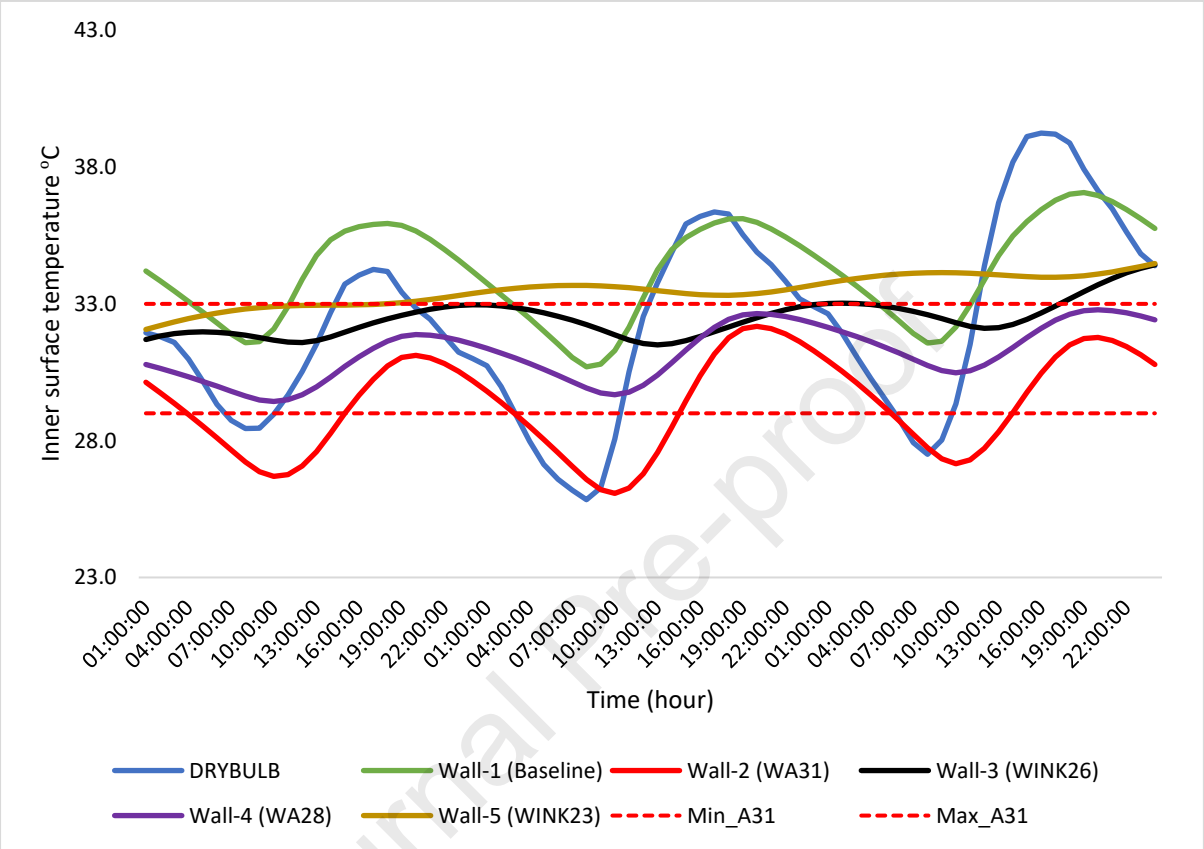

Fig. 15 Inner surface temperature for PCM A31, A28, Inertek26, and Inertek23

Table 6 Inner surface temperature reduction of PCM A31, A28, Inertek26, and Inertek23

DAYS	**A31 TEMP℃**	**A28 TEMP℃**	**INERTEK26 TEMP℃**	**INERTEK23 TEMP℃**
18TH APRIL	4.8	4.0	3.1	2.3
19TH APRIL	4.0	4.4	3.2	2.0
20TH APRIL	5.3	4.3	3.7	2.5

5.2.1.2. The Effect of PCM Layer Thickness on Inner Wall Surface Temperature

The capacity of PCM is based on the extent to which it can go through a full-phase cycle in one day. The required thickness was determined by varying the PCM layer thickness from 1cm to 7cm. The temperature variation for the PCM-integrated earthbag unit wall with various PCM thicknesses in April is shown in Fig. 16 and Fig. 17. It is evident that the inner wall temperature shifts drastically when solar radiation is present and when the external air temperature varies. It was determined that when the PCM layer thickness was increased from 1 to 7 cm, the maximum temperature of the inner wall decreased significantly. For instance, for Wall-2 (WA31), as shown in Fig. 17, the maximum temperature of the wall with a 1 cm layer thickness is 35.1℃, while for a 6 cm layer, it is 31.7℃, exhibiting a considerable difference of 3.4℃. Likewise, for Wall-3 (WInk26), as depicted in **Fig. *17***, the temperature difference between the 1 cm and 7 cm layers is approximately 1.5℃.

Moreover, the wall with a 6 cm layer of A31 and a 7 cm layer of Inertek26 demonstrates a remarkable thermal performance with an average maximum peak temperature reduction of 3.1℃ and 1.7℃, respectively, over the three days compared to the wall reinforced by a 1 cm PCM layer. Moreover, comparing Wall-2 (WA31) and Wall-1 (baseline), the temperature reduction was found to be 4.0℃. This is likely because a thicker PCM layer has a greater capacity to store heat energy and shows greater thermal inertia, thus reducing the variation in the indoor wall surface temperature during the test. However, when the PCM layer was increased to 7 cm for Wall-2 (WA31), the temperature amplitude increased above the values for all other PCM layers. This is because when the PCM layer is too thick, the PCM may not solidify and thus act as an additional layer to the wall rather than as an energy storage [71].

The impact of the thickness of the PCM layer on PCM charging and discharging capacities is further investigated in this study. By determining the inner-surface temperature of the earthbag wall, it is possible to estimate whether the phase change material is in a solid or liquid state. The results of the charging and discharging of the PCM in Wall-2 (WA31) are positive for the 6 cm PCM layer, as illustrated in the charging and discharging area in **Fig. *16***. On the first day, the wall surface temperature remained below the melting temperature of the PCM for 10 h (04:00 to 14:00) and above the melting temperature for 14 h (15:00 to 5:00), giving the PCM time to charge and discharge, respectively. The results demonstrated that the PCM provided effective thermal regulation, allowing the wall surface temperature to remain within the desired range, thus providing a comfortable living environment in the building. On the second and third days, the charging and discharging hours were 9,7, and, 15, and 17 h, respectively. However, on the third day, there was insufficient time for the PCM to charge, making it ineffective. Wall-'3's (WInk26) inner surface temperature analysis, shown in Fig. 17 with

different PCM layer thicknesses, demonstrates that the PCM is ineffective as an energy storage technology because the inner surface temperature is consistently above the melting temperature of the PCM. Therefore, the PCM acts only as an additional layer to increase the thermal inertia. Hence, based on the analysis above, Wall-2 (WA31) with a 6 cm PCM layer of A31 is more effective than that of the Wall-3 (WInk26) wall in all layers (1–7 cm).

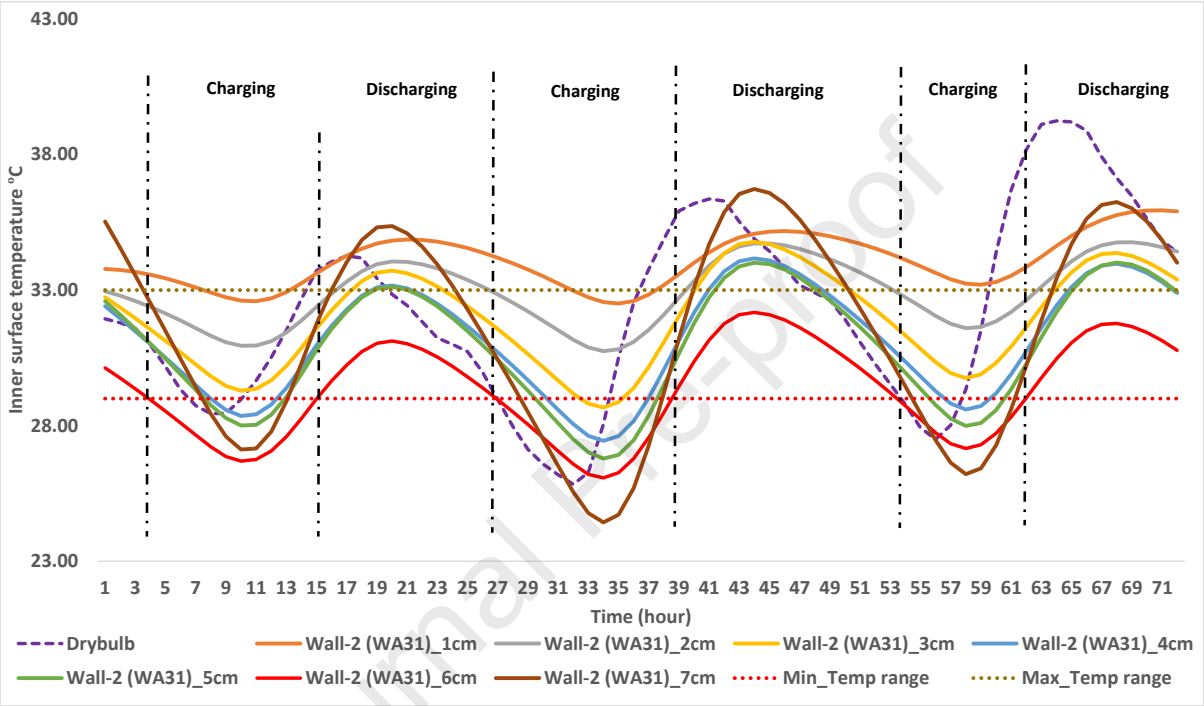

Fig. 16 Inner wall surface temperature of Wall-2 (WA31)

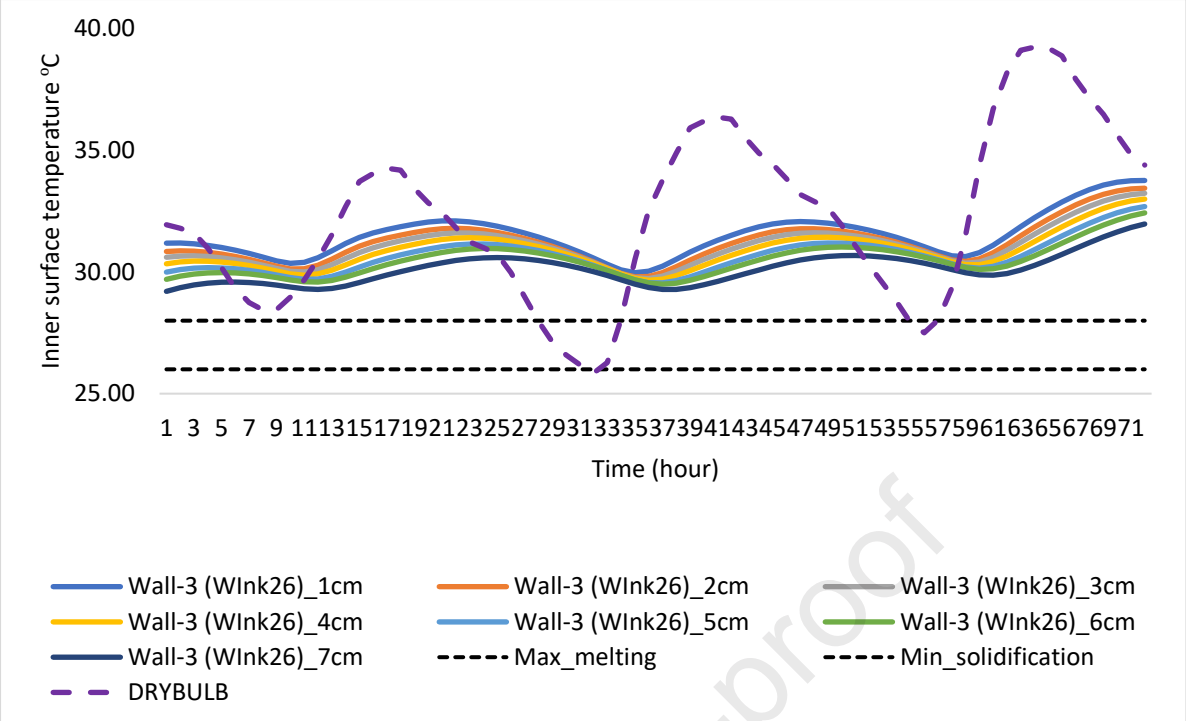

Fig. 17 Inner wall surface temperature of Wall-3 (WInk26)

5.2.1.3. The Effect of PCM Layer Location

This study also examined the impact of the PCMs layer location on the thermal performance of earthbag-building models. Two scenarios were considered: PCM layers were placed on the exterior and interior surfaces of the earthbag walls. The results indicate that the performance of the PCM layer varies depending on its location on the wall. When the PCM layer was placed on the exterior surface of the earthbag wall, there was a temperature reduction on the first day for all walls considered, with Wall-2 exhibiting the highest reduction of 2.1°C as shown in Fig. 18. However, on the second and third days, the temperature reduction decreased for all walls, which even recorded negative temperature reductions, implying that the earthbag wall without PCM performed better than the wall with the PCM layer.

However, when the PCM layer was placed on the interior surface of the earthbag wall, all walls recorded temperature reductions on all three days. Wall-2 exhibited the highest temperature reduction of 5.3°C on the third day. At the same time, wall-2 had the lowest temperature reduction of 4.0°C on the second day. Wall-3 and wall-5 had temperature reductions ranging from 2.0°C to 3.7°C, as shown in Fig. 19. The results showed that the location of the PCM layer in the earthbag wall models significantly affected the thermal performance. PCM layers placed on the exterior surface of the wall may not be effective in reducing the temperature of the wall. In contrast, PCM layers placed on the interior surface of the wall can significantly reduce the temperature.

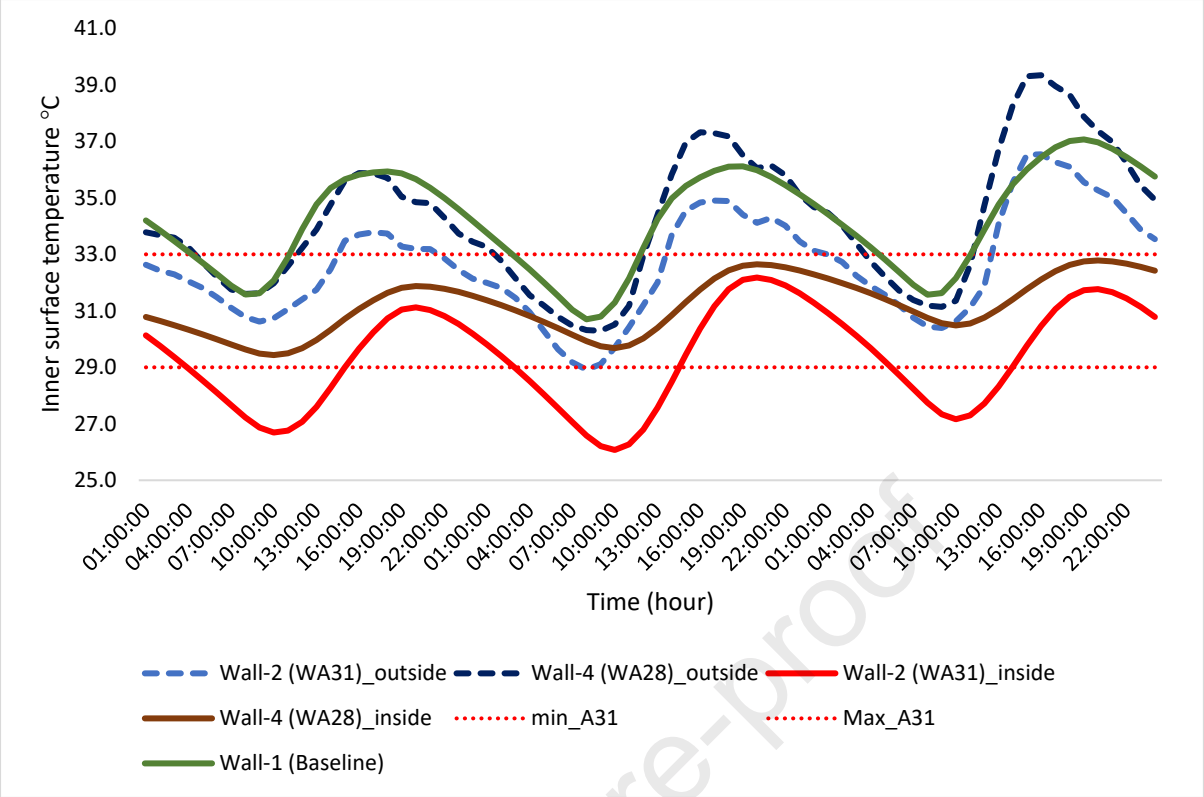

730

731 **Fig. 18** Inner wall surface temperature of A31 PCM layer in a different layer position

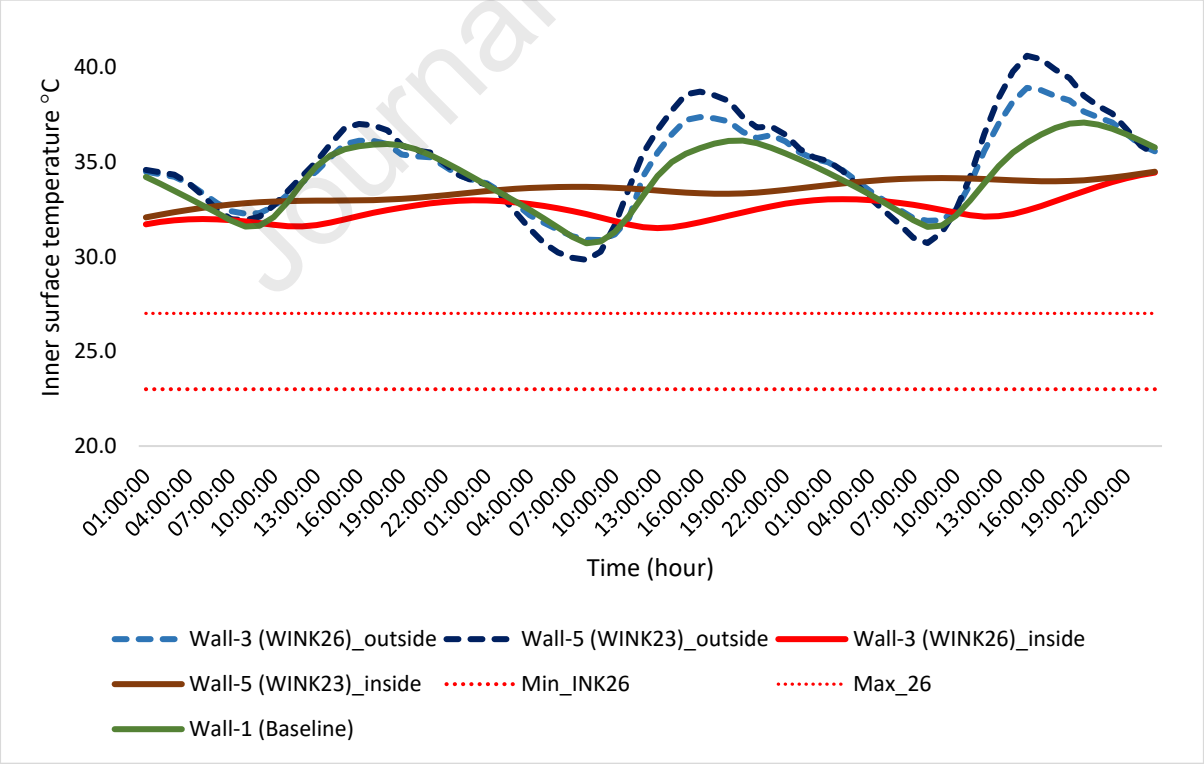

732

733

734 **Fig. 19** inner wall surface temperature of Inertek26 PCM layer in a different layer position

6. Conclusion

The utilisation of thermal energy storage systems using phase change materials in conventional buildings, such as concrete and steel, has been identified as a reliable and resourceful energy technology for improving the efficiency and sustainability of buildings. The study presents a novel approach by incorporating PCM into earthbag building practices, addressing a significant gap in research related to thermal comfort in temporary housing, particularly in hot climates like Nigeria. The limited exploration of PCM in building materials and the general oversight of its benefits in traditional vernacular building methods highlight the study's innovative nature. This research is pivotal in examining the thermal properties and characteristics of earth buildings integrated with PCM, a subject not extensively studied previously. The study's experimental component involved incorporating paraffin wax and microencapsulated PCM into scaled-down earthbag walls, with performance evaluated in a controlled environment. The findings, validated against a numerical simulation model in EnergyPlus, showed significant thermal improvements with PCM integration. The main conclusions of this study are as follows:

- The results from the experiment revealed that Wall-3 (WInk26) is an effective wall in terms of heat transfer compared with Wall-2 (WA31) and Wall-1 (baseline). This is evidenced by the average amount of heat transfer from the outer surface to the interior surface of Wall-1 (baseline), which is found to be 227 $Wh/\,m^2$ throughout the experiment. This value is substantially higher than that of Wall-2 (WA31), with a value of 81.24 $Wh/\,m^2$ and Wall-3 (WInk26) with a value of 49.2 $Wh/\,m^2$.
- PCM effectively reduced the heat flux penetration with Wall-3 (WInk26), which displayed the highest performance of 63.76% compared with Wall-2 (WA31) at 39.34%. This suggests that the average heat flux reduction varies significantly depending on the type of PCM, making Inertek26 a suitable choice for achieving a thermal comfort range. However, despite the acceptable performance of Wall-3 (WInk26), Inertek26 did not show a positive result regarding PCM charging and discharging. Hence, parametric analysis is conducted to determine the best functional PCM.
- The simulation model was successfully validated as various performance criteria were aligned within an acceptable range. The experimentally and numerically measured temperatures displayed similar patterns. The temperature profiles are consistent with the modelling results, and only minor changes can be observed between the numerical and experimental studies.
- Our findings has established that PCMA31 was found to be optimum for buildings in the Kano state and similar climatic conditions. Increasing the PCM layer thickness from 1 to 7 cm significantly reduced the maximum temperature of the inner wall surface. However, when the

PCM layer was too thick, it acted as an additional layer to the wall rather than as an energy storage technology.

- Additionally, the parametric study found that incorporating a 6 cm PCM layer into the earthbag wall (Wall-2) is the optimum thickness for reducing the inner wall temperature. This resulted in a temperature reduction of 4.0℃ compared to the baseline (Wall-1). In contrast, Wall-3, which had an Inertek26 PCM layer ranging from 1 cm to 7 cm, did not actively charge and discharge the PCM, leading to a comparatively lower temperature reduction of 3.1℃. Overall, the study concluded that PCM integration effectively reduces indoor wall surface temperature variations and creates a comfortable living environment in buildings.

Overall In comparison to other literature findings concerning the impact of Phase Change Materials (PCM) on thermal discomfort reduction in vernacular buildings, our research highlights promising outcomes. Incorporating PCM into earthbag walls, such as paraffin wax A31 and microencapsulation Inertek26, yielded significant surface temperature reductions. This aligns with prior research by Sandra et al. (2022) [72] on PCM in compacted earth blocks, Serrano et al. (2013) [39] on stabilized rammed earth, and Gounni & Louahlia (2020) [40] on PCM-integrated cob houses, all indicating enhanced thermal performance. Furthermore, Toufigh and Samadianfard (2022) [42] demonstrated PCM's potential in controlling temperature variations in rammed earth, echoing our findings.

7. Limitations and Future Research

The study has some limitations that need to be addressed in the future. First, the study does not take into consideration of a hysteresis effect when simulating the surface temperature of earthbag unit. This could be a concern if you want to simulate variation in surface temperature throughout a year. Future research can address this problem by integrating the hysteresis effect within the model. Future research should also comprehensively evaluate the technical and economic aspects of the proposed PCM-integrated earthbag unit model. The social acceptance of PCM-integrated earthbag units should be conducted to prove the sustainability and affordability of this building model. The structural integrity and effectiveness of the PCM-integrated earthbag units should also be studied. The performance analysis of PCM-integrated earthbag units should be conducted in different climates. Additionally, limiting the overall analysis to a brief period of three days, emphasizing the need for future studies to expand the temporal scope, to capture diverse seasonal variations and enhance understanding of year-round thermal comfort in varying climatic conditions.

CRediT authorship contribution statement

Mahmoud Murtala Farouq: Conceptualization, Writing – original draft, Software, Formal analysis, Investigation. **Parham A Mirzaei**: Writing – review & editing, Supervision, Visualisation. **Carlos Jimenez-Bescos**: Writing – review & editing, Supervision. **Saffa Riffat**: Writing – review & editing, Supervision.

Declaration of competing interests

The authors declare that they have no known competing financial interests or personal relationships that could have appeared to influence the work reported in this paper.

Data availability

Data will be made available on request.

Acknowledgements

The authors would like to thank the Faculty of Engineering at The University of Nottingham for their assistance on the research project. Furthermore, they wish to express their appreciation to the Petroleum Technology Development Fund (PTDF) of Nigeria for funding this study through Grant No. **PTDF/ED/OSS/PHD/MFM/1619/19**.

Appendix A

Fig. A. 1 Earthbag block mould

Appendix B

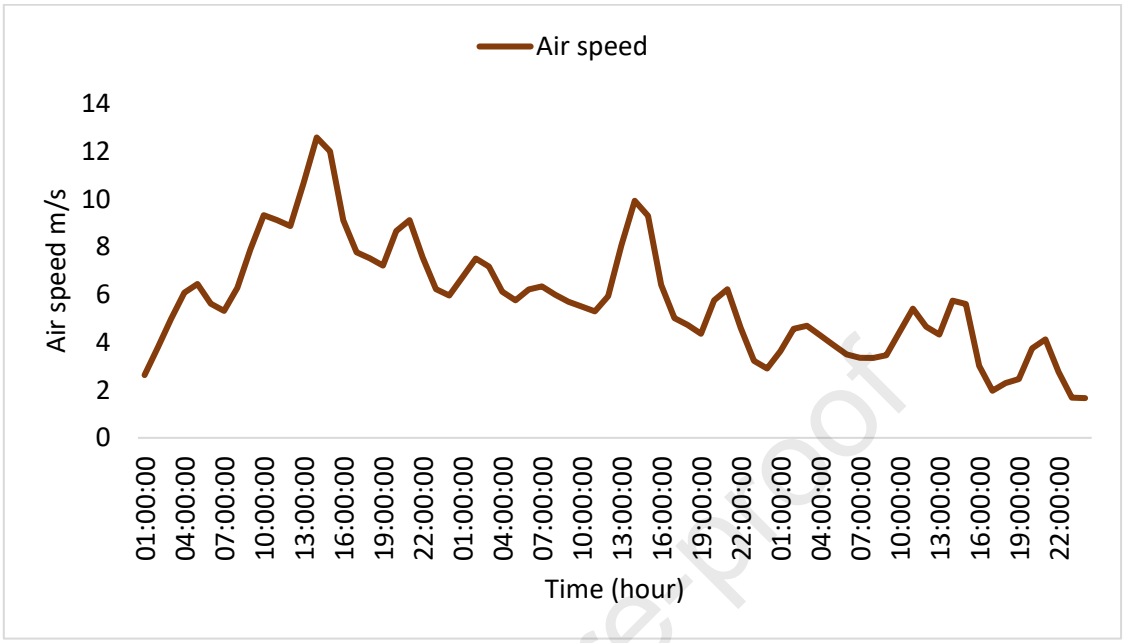

Fig. B. 1 Air speed in a typical summer day in Kano state

Appendix C

In this study, it was determined that the amount of phase change material (PCM) used in each earthbag unit block was 2.2% of the total block volume, as outlined in Section 2.1.2. The actual weight of the PCM found in each block was 0.39 kg. To calculate the thickness of the PCM layer in the block, the density of the PCM from **Table *1*** was used, along with the dimensions of a single earthbag block shown in Fig. C. 1 Fig. C. 1.

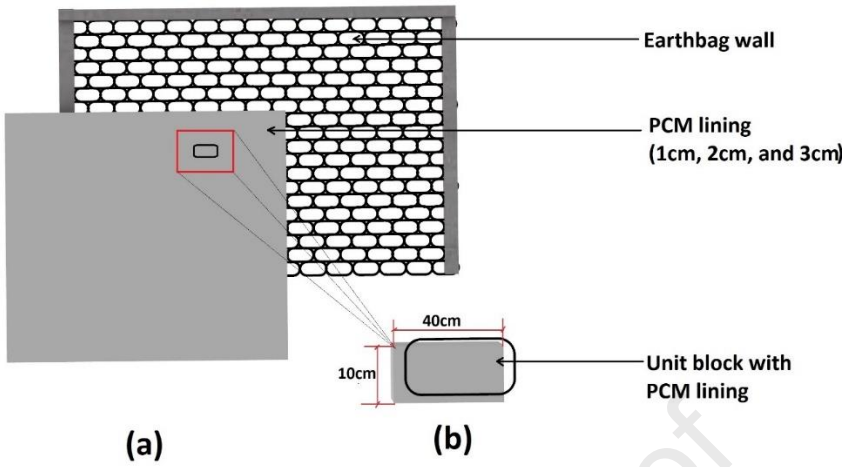

832

833 **Fig. C. 1** (a) PCM lining thickness on the earthbag wall (b) PCM lining on the earthbag block

834 By applying the PCM equivalent method, the thickness of the PCM layer was calculated using A. 1
835 below:

$$Thickness = Mass / (length\ x\ width\ x\ density) \quad A.\ 1$$

836 $$Thickness = 0.39\ kg / (0.1\ m\ x\ 0.4\ m\ x\ 860\ kg/m^3)$$

837 $$Thickness \approx 0.011\ m\ or\ 11mm$$

838

839

840

841

842

843

844

845

Reference

[1] J. Milano *et al.*, "Microalgae biofuels as an alternative to fossil fuel for power generation," *Renew. Sustain. Energy Rev.*, vol. 58, pp. 180–197, 2016, doi: 10.1016/j.rser.2015.12.150.

[2] N. M. A. Mutombo and B. P. Numbi, "Assessment of renewable energy potential in Kwazulu-Natal province, South Africa," *Energy Reports*, vol. 5, pp. 874–881, 2019, doi: 10.1016/j.egyr.2019.07.003.

[3] A. Chel and G. Kaushik, "Renewable energy technologies for sustainable development of energy efficient building," *Alexandria Eng. J.*, 2017, doi: 10.1016/j.aej.2017.02.027.

[4] J. Liu, X. Chen, S. Cao, and H. Yang, "Overview on hybrid solar photovoltaic-electrical energy storage technologies for power supply to buildings," *Energy Convers. Manag.*, vol. 187, no. December 2018, pp. 103–121, 2019, doi: 10.1016/j.enconman.2019.02.080.

[5] C. Chidebell-Emordi, "The African electricity deficit: Computing the minimum energy poverty line using field research in urban Nigeria," *Energy Res. Soc. Sci.*, vol. 5, pp. 9–19, 2015, doi: 10.1016/j.erss.2014.12.011.

[6] S. Adewale, "Internally displaced persons and the challenges of survival in Abuja," *African Secur. Rev.*, vol. 25, no. 2, pp. 176–192, 2016, doi: 10.1080/10246029.2016.1154475.

[7] N. M. Gwadabe, M. A. Salleh, A. A. Ahmad, and S. Jamil, "Forced Displacement and the Plight of Internally Displaced Persons in Northeast Nigeria," *Humanit. Soc. Sci. Res.*, vol. 1, no. 1, p. p46, 2018, doi: 10.30560/hssr.v1n1p46.

[8] R. Kamal and M. S. Rahman, "A study on feasibility of super adobe technology -an energy efficient building system using natural resources in Bangladesh," *IOP Conf. Ser. Earth Environ. Sci.*, vol. 143, no. 1, 2018, doi: 10.1088/1755-1315/143/1/012043.

[9] I. O. Olufemi, S. Sule, and S. Ibrahim, "Mainstreaming Protection in Internally Displaced Persons Camp in Mainstreaming Protection in Internally Displaced Persons Camp in Maiduguri , Borno State , Nigeria," no. February, 2020, doi: 10.9790/0837-2502053443.

[10] E. Alobo and S. Obaji, "Internal Displacement in Nigeria and the Case for Human Rights Protection of Displaced Persons," *J. Law, Policy Glob.*, vol. 51, no. 3, pp. 26–33, 2016.

[11] S. Ekpa and N. H. M. Dahlan, "Legal Issues and Prospects in the Protection and Assistance of Internally Displaced Persons (IDPs) in Nigeria," *J. Law, Policy Glob.*, vol. 49, no. 0, pp. 108–116, 2016, [Online]. Available: https://www.iiste.org/Journals/index.php/JLPG/article/view/30769/31596

[12] O. Eweka and T. O. Olusegun, "Management of Internally Displaced Persons in Africa: Comparing Nigeria and Cameroon," *African Res. Rev.*, vol. 10, no. 1, p. 193, 2016, doi: 10.4314/afrrev.v10i1.15.

[13] A.-S. M. A.-S. Samara and S. Rasha Mahmoud, Ali Al Zaini, Mohamed, "The Cosmic House (a case study of a sustainable Earthbag house) in Jordan," *J. Arts Humanit.*, vol. 4, no. 8, pp. 241–253, 2021, doi: 10.21608/mjas.2022.102230.1038.

[14] L. Rincón, A. Carrobé, M. Medrano, C. Solé, A. Castell, and I. Martorell, "Analysis of the thermal behavior of an earthbag building in Mediterranean continental climate: Monitoring and simulation," *Energies*, vol. 13, no. 1, 2019, doi: 10.3390/en13010162.

[15] L. Rincón, A. Carrobé, I. Martorell, and M. Medrano, "Improving thermal comfort of earthen dwellings in sub-Saharan Africa with passive design," *J. Build. Eng.*, vol. 24, no. April, p.

100732, 2019, doi: 10.1016/j.jobe.2019.100732.

[16] R. Wesonga, H. Kasedde, N. Kibwami, and M. Manga, “A Comparative Analysis of Thermal Performance, Annual Energy Use, and Life Cycle Costs of Low-cost Houses Made with Mud Bricks and Earthbag Wall Systems in Sub-Saharan Africa,” *Energy Built Environ.*, no. June, 2021, doi: 10.1016/j.enbenv.2021.06.001.

[17] A. Castell, S. Vall, A. Carrobé, M. Medrano, I. Martorell, and L. Rincón, “Radiative Cooling to Cover Cooling Demands of an Earthbag Building in a Training Medical Cernter in Burkina Faso,” no. Hunter 2004, pp. 1–6, 2019, doi: 10.18086/eurosun2018.06.03.

[18] R. Kamal and M. S. Rahman, “A study on feasibility of super adobe technology -an energy efficient building system using natural resources in Bangladesh,” in *IOP Conference Series: Earth and Environmental Science*, 2018, vol. 143, no. 1. doi: 10.1088/1755-1315/143/1/012043.

[19] U. Desideri, S. Proietti, P. Sdringola, and E. Vuillermoz, “Feasibility study and design of a low-energy residential unit in Sagarmatha park for environmental impact reduction of high altitude buildings,” *Proc. 25th Int. Conf. Effic. Cost, Optim. Simul. Energy Convers. Syst. Process. ECOS 2012*, vol. 7, pp. 173–185, 2012.

[20] M. Theodoridou, L. Kyriakou, and I. Ioannou, “PCM-enhanced Lime Plasters for Vernacular and Contemporary Architecture,” *Energy Procedia*, vol. 97, pp. 539–545, 2016, doi: 10.1016/j.egypro.2016.10.070.

[21] Y. Kang, S. G. Jeong, S. Wi, and S. Kim, “Energy efficient Bio-based PCM with silica fume composites to apply in concrete for energy saving in buildings,” *Sol. Energy Mater. Sol. Cells*, vol. 143, pp. 430–434, 2015, doi: 10.1016/j.solmat.2015.07.026.

[22] P. A. Mirzaei and F. Haghighat, “Modeling of phase change materials for applications in whole building simulation,” *Renew. Sustain. Energy Rev.*, vol. 16, no. 7, pp. 5355–5362, 2015, doi: 10.1016/j.rser.2012.04.053.

[23] A. Al Touma and D. Ouahrani, “Improved human thermal comfort with indoor PCM-Enhanced tiles in living spaces in the arabian gulf,” *E3S Web Conf.*, vol. 57, 2018, doi: 10.1051/e3sconf/20185704001.

[24] Y. Zhou *et al.*, “Passive and active phase change materials integrated building energy systems with advanced machine-learning based climate-adaptive designs, intelligent operations, uncertainty-based analysis and optimisations: A state-of-the-art review,” *Renew. Sustain. Energy Rev.*, vol. 130, no. April, p. 109889, 2020, doi: 10.1016/j.rser.2020.109889.

[25] M. Velasco-Carrasco, O. Ramadan, and S. Riffat, “Experimental Study of PCM Cooling Storage System for Hot Climates,” *Futur. Cities Environ.*, vol. 8, no. 1, pp. 1–11, 2022, doi: 10.5334/fce.148.

[26] K. Liu, Z. Yuan, H. Zhao, C. Shi, and F. Zhao, “Properties and Applications of Shape-Stabilized Phase Change Energy Storage Materials Based on Porous Material Support—A review,” *Mater. Today Sustain.*, vol. 21, p. 100336, 2023, doi: 10.1016/j.mtsust.2023.100336.

[27] S. Ramakrishnan, J. Sanjayan, X. Wang, M. Alam, and J. Wilson, “A novel paraffin/expanded perlite composite phase change material for prevention of PCM leakage in cementitious composites,” *Appl. Energy*, vol. 157, pp. 85–94, 2015, doi: 10.1016/j.apenergy.2015.08.019.

[28] S. Hasanabadi, S. M. Sadrameli, H. Soheili, H. Moharrami, and M. M. Heyhat, “A cost-effective form-stable PCM composite with modified paraffin and expanded perlite for thermal energy storage in concrete,” *J. Therm. Anal. Calorim.*, vol. 136, no. 3, pp. 1201–1216, 2019, doi:

10.1007/s10973-018-7731-8.

[29] P. Lv, M. Ding, C. Liu, and Z. Rao, “Experimental investigation on thermal properties and thermal performance enhancement of octadecanol/expanded perlite form stable phase change materials for efficient thermal energy storage,” *Renew. Energy*, vol. 131, pp. 911–922, 2019, doi: 10.1016/j.renene.2018.07.102.

[30] H. Cui, S. A. Memon, and R. Liu, “Development, mechanical properties and numerical simulation of macro encapsulated thermal energy storage concrete,” *Energy Build.*, vol. 96, pp. 162–174, 2015, doi: 10.1016/j.enbuild.2015.03.014.

[31] X. Mi, R. Liu, H. Cui, S. A. Memon, F. Xing, and Y. Lo, “Energy and economic analysis of building integrated with PCM in different cities of China,” *Appl. Energy*, vol. 175, pp. 324–336, 2016, doi: 10.1016/j.apenergy.2016.05.032.

[32] S. Ramakrishnan, X. Wang, J. Sanjayan, and J. Wilson, “Thermal performance assessment of phase change material integrated cementitious composites in buildings: Experimental and numerical approach,” *Appl. Energy*, vol. 207, pp. 654–664, 2017, doi: 10.1016/j.apenergy.2017.05.144.

[33] S. Kenzhekhanov, S. A. Memon, and I. Adilkhanova, “Quantitative evaluation of thermal performance and energy saving potential of the building integrated with PCM in a subarctic climate,” *Energy*, vol. 192, p. 116607, 2020, doi: 10.1016/j.energy.2019.116607.

[34] I. Adilkhanova, S. A. Memon, J. Kim, and A. Sheriyev, “A novel approach to investigate the thermal comfort of the lightweight relocatable building integrated with PCM in different climates of Kazakhstan during summertime,” *Energy*, vol. 217, p. 119390, 2021, doi: 10.1016/j.energy.2020.119390.

[35] A. Louanate, R. El Otmani, K. Kandoussi, and M. Boutaous, “Dynamic modeling and performance assessment of single and double phase change material layer–integrated buildings in Mediterranean climate zone,” *J. Build. Phys.*, vol. 44, no. 5, pp. 461–478, 2021, doi: 10.1177/1744259120945361.

[36] H. El Fakiri, L. Ouhsaine, and A. El Bouardi, “Thermal Dynamic Behavior in Bi-Zone Habitable Cell with and without Phase Change Materials,” *Proceedings*, vol. 63, no. 1, p. 41, 2020, doi: 10.3390/proceedings2020063041.

[37] R. Saxena, D. Rakshit, and S. C. Kaushik, “Phase change material (PCM) incorporated bricks for energy conservation in composite climate: A sustainable building solution,” *Sol. Energy*, vol. 183, no. March, pp. 276–284, 2019, doi: 10.1016/j.solener.2019.03.035.

[38] L. Erlbeck *et al.*, “Adjustment of thermal behavior by changing the shape of PCM inclusions in concrete blocks,” *Energy Convers. Manag.*, vol. 158, no. October 2017, pp. 256–265, 2018, doi: 10.1016/j.enconman.2017.12.073.

[39] S. Serrano, C. Barreneche, L. Rincón, D. Boer, and L. F. Cabeza, “Optimization of three new compositions of stabilized rammed earth incorporating PCM: Thermal properties characterization and LCA,” *Constr. Build. Mater.*, vol. 47, pp. 872–878, 2013, doi: 10.1016/j.conbuildmat.2013.05.018.

[40] A. Gounni and H. Louahlia, “Dynamic behavior and economic analysis of sustainable building integrating cob and phase change materials,” *Constr. Build. Mater.*, vol. 262, p. 120795, 2020, doi: 10.1016/j.conbuildmat.2020.120795.

[41] Z. Ben Zaid, A. Tilioua, I. Lamaamar, O. Ansari, H. Souli, and M. A. Hamdi Alaoui, “An experimental study of the efficacy of integrating a phase change material into a clay-straw

wall in the Drâa-Tafilalet Region (Errachidia Province), Morocco," *J. Build. Eng.*, vol. 32, no. January, 2020, doi: 10.1016/j.jobe.2020.101670.

[42] V. Toufigh and S. Samadianfard, "Experimental and numerical investigation of thermal enhancement methods on rammed-earth materials," *Sol. Energy*, vol. 244, no. August 2021, pp. 474–483, 2022, doi: 10.1016/j.solener.2022.08.049.

[43] Y. M'hamdi, K. Baba, M. Tajayouti, and A. Nounah, "Energy, environmental, and economic analysis of different buildings envelope integrated with phase change materials in different climates," *Sol. Energy*, vol. 243, no. July, pp. 91–102, 2022, doi: 10.1016/j.solener.2022.07.031.

[44] M. M. Farouq, C. Jimenez-bescos, S. Riffat, and P. A. Mirzaei, "Development and thermal characteristic study of an integrated phase change material earthbag unit for temporary building," *Energy Build.*, no. xxxx, 2023.

[45] A. Batagarawa, "Assessing the thermal performance of phase change materials in composite hot humid / hot dry climates: An examination of office buildings in Abuja- Nigeria," 2013.

[46] S. Ali, B. Martinson, and S. Al-Maiyah, "Evaluating neutral , preferred , and comfort range temperatures and computing adaptive equation for Kano region computing adaptive equation for Kano region," 2020.

[47] MCI Technologies and Winco Technologies, "INERTEK Microcapsules," France, 2012. [Online]. Available: https://www.winco-tech.com/en/produit/inertek-2/

[48] P. C. M. Products, "PlusICE® Organic Range." [Online]. Available: www.pcmproducts.net

[49] MCI, "The MCI Technologies company," 2017.

[50] D. M. dos Santos and J. N. D. C. Beirão, "Generative tool to support architectural design decision of earthbag building domes," 2017, no. November, pp. 538–543. doi: 10.5151/sigradi2017-083.

[51] GEG, "How to Build an Earthquake-Resistant Home: An Earthbag Construction Manual," *Good Earth Global*, 2018.

[52] A. Tokuç, T. Başaran, and S. C. Yesügey, "An experimental and numerical investigation on the use of phase change materials in building elements: The case of a flat roof in Istanbul," *Energy Build.*, vol. 102, pp. 91–104, 2015, doi: 10.1016/j.enbuild.2015.04.039.

[53] T. Sensors, "HFP01 Heat flux plate / heat flux sensor," 2014. [Online]. Available: https://www.hukseflux.com/uploads/product-documents/HFP01_v2114.pdf

[54] A. Hasan, K. A. Al-Sallal, H. Alnoman, Y. Rashid, and S. Abdelbaqi, "Effect of phase change materials (PCMs) integrated into a concrete block on heat gain prevention in a hot climate," *Sustain.*, vol. 8, no. 10, 2016, doi: 10.3390/su8101009.

[55] Q. Al-Yasiri and M. Szabó, "Thermal performance of concrete bricks based phase change material encapsulated by various aluminium containers: An experimental study under Iraqi hot climate conditions," *J. Energy Storage*, vol. 40, no. May, 2021, doi: 10.1016/j.est.2021.102710.

[56] S. Shaik, K. K. Gorantla, and A. B. T. P. Setty, "Investigation of Building Walls Exposed to Periodic Heat Transfer Conditions for Green and Energy Efficient Building Construction," *Procedia Technol.*, vol. 23, pp. 496–503, 2016, doi: 10.1016/j.protcy.2016.03.055.

[57] N. Soares, A. R. Gaspar, P. Santos, and J. J. Costa, "Multi-dimensional optimization of the

incorporation of PCM-drywalls in lightweight steel-framed residential buildings in different climates," *Energy Build.*, vol. 70, pp. 411–421, 2014, doi: 10.1016/j.enbuild.2013.11.072.

[58] M. Özdenefe, U. Atikol, and M. Rezaei, "Trombe wall size-determination based on economic and thermal comfort viability," *Sol. Energy*, vol. 174, no. September, pp. 359–372, 2018, doi: 10.1016/j.solener.2018.09.033.

[59] P. C. Tabares-Velasco, C. Christensen, and M. Bianchi, "Verification and validation of EnergyPlus phase change material model for opaque wall assemblies," *Build. Environ.*, vol. 54, pp. 186–196, 2012, doi: 10.1016/j.buildenv.2012.02.019.

[60] P. C. Tabares-Velasco, C. Christensen, and M. Bianchi, "Verification and validation of EnergyPlus phase change material model for opaque wall assemblies," *Build. Environ.*, vol. 54, no. July, pp. 186–196, 2012, doi: 10.1016/j.buildenv.2012.02.019.

[61] Y. Sang, J. R. Zhao, J. Sun, B. Chen, and S. Liu, "Experimental investigation and EnergyPlus-based model prediction of thermal behavior of building containing phase change material," *J. Build. Eng.*, vol. 12, no. March, pp. 259–266, 2017, doi: 10.1016/j.jobe.2017.06.011.

[62] A. AbdulKadir, M. T. Usman, and A. H. Shaba, "An integrated approach to delineation of the eco-climatic zones in Northern Nigeria," *J. Ecol. Nat. Environ.*, vol. 7, no. 9, pp. 247–255, 2015, doi: 10.5897/jene2015.0532.

[63] O. K. Akande, "Passive design strategies for residential buildings in a hot dry climate in Nigeria," *WIT Trans. Ecol. Environ.*, vol. 128, pp. 61–71, 2010, doi: 10.2495/ARC100061.

[64] S. Guichard, F. Miranville, D. Bigot, B. Malet-Damour, T. Libelle, and H. Boyer, "Empirical validation of a thermal model of a complex roof including phase change materials," *Energies*, vol. 9, no. 1, 2016, doi: 10.3390/en9010009.

[65] Á. Lakatos, "Comparison of the thermal properties of different insulating materials," *Adv. Mater. Res.*, vol. 899, no. February, pp. 381–386, 2014, doi: 10.4028/www.scientific.net/AMR.899.381.

[66] A. V. Sá, M. Azenha, H. De Sousa, and A. Samagaio, "Thermal enhancement of plastering mortars with Phase Change Materials: Experimental and numerical approach," *Energy Build.*, vol. 49, pp. 16–27, 2012, doi: 10.1016/j.enbuild.2012.02.031.

[67] K. Faraj, M. Khaled, J. Faraj, F. Hachem, and C. Castelain, "A review on phase change materials for thermal energy storage in buildings: Heating and hybrid applications," *J. Energy Storage*, vol. 33, no. June 2020, p. 101913, 2021, doi: 10.1016/j.est.2020.101913.

[68] J. Yu, K. Leng, F. Wang, H. Ye, and Y. Luo, "Simulation study on dynamic thermal performance of a new ventilated roof with form-stable pcm in Southern China," *Sustain.*, vol. 12, no. 22, pp. 1–21, 2020, doi: 10.3390/su12229315.

[69] R. Saxena, D. Rakshit, and S. C. Kaushik, "Experimental assessment of Phase Change Material (PCM) embedded bricks for passive conditioning in buildings," *Renew. Energy*, vol. 149, pp. 587–599, 2020, doi: 10.1016/j.renene.2019.12.081.

[70] Y. Rashid, F. Alnaimat, and B. Mathew, "Energy performance assessment of waste materials for buildings in extreme cold and hot conditions," *Energies*, vol. 11, no. 11, 2018, doi: 10.3390/en11113131.

[71] K. S. Reddy, V. Mudgal, and T. K. Mallick, "Thermal performance analysis of multi-phase change material layer-integrated building roofs for energy efficiency in built-environment," *Energies*, vol. 10, no. 9, 2017, doi: 10.3390/en10091367.

[72] C. Sandra, C. André, J. Aguiar, and M. Francisco, “Compacted Earth Blocks Additivated with Phase Change Material,” *Sci. Electron. Libr. Online*, vol. 2, p. 27, 2022.

Highlights

PCM-earthbag walls reduces surface temperatures, enhancing thermal comfort

Paraffin Wax A31 is the optimal PCM due to its transition temperature

PCM at interior surface wall shows a better thermal comfort

Study highlights PCM-earthbag synergy for improved thermal comfort

Mahmoud Murtala Farouq: Methodology, Investigation, Software, Validation, Writing - original draft

Parham A. Mirzaei: Conceptualization, Methodology, Supervision, Writing - review & editing

Carlos Jimenez-Bescos: Conceptualization, Methodology, Supervision, Writing - review & editing

Saffa Riffat: Supervision, Writing - review & editing

Declaration of interests

☒ The authors declare that they have no known competing financial interests or personal relationships that could have appeared to influence the work reported in this paper.

☐The authors declare the following financial interests/personal relationships which may be considered as potential competing interests: